POLITECNICO
MILANO 1863

SCUOLA DI INGEGNERIA INDUSTRIALE
E DELL'INFORMAZIONE

Two dimensional electron spectroscopy of graphene nanoribbons: modeling and experiment

Tesi di Laurea Magistrale in
Engineering Physics - Ingegneria Fisica

Author: **Giacomo Bassi**

Student ID: 997204
Advisor: Prof. Margherita Maiuri
Co-advisors: Mattia Russo
Academic Year: 2022-2023

Abstract

Nanographenes are promising nanostructure that can be engineered and design to tailor their properties for a specific use. The confinement of graphene within a few nanometers has led to the creation of a finite band gap in its electronic structure. This development opened for nanographenes a variety of applications with promising results [1]. This Thesis focuses on Dibenzo[hi,st]ovalene molecule functionalized with two mesityl groups and two chlorine atoms (DBOVMes-Cl). The study focuses on its optoelectronic properties and on the interplay between electronic photo-excitation and vibrational degree of freedom. Such analysis was made possible by advance ultrafast spectroscopy techniques. Two-dimensional electron spectroscopy (2DES) emerges as a powerful time-resolved spectroscopical tool, offering high temporal and frequency resolution. The modeling of the experiment and its simulation were contextually developed allowing conjectures about the origin and role of molecular excited and ground state vibrations. The Brownian oscillator model and the displaced oscillator model were merged and applied to a two levels system to simulate a full 2DES dataset. The simulation were able to predict the lineshape evolution and the signal dynamics so that the defining physical quantities could be inferred from the model parameters. Additionally the presented evidences argue for a greater involvement of the excited state to the vibrational mode in the respect to the ground state. This can have profound implications in processes like energy and charges transfer within the molecule

Keywords: nanographenes, two dimensional electronic spectroscopy, vibronic coupling, Brownian oscillators, displaced oscillators

Abstract in lingua italiana

I nanografeni sono promettenti nanostrutture che possono essere progettate e ingegnerizzate per adattare le loro proprietà a un uso specifico. Il confinamento del grafene entro pochi nanometri ha portato alla creazione di salti energetici finiti nella sua struttura elettronica. Questo sviluppo ha aperto per i nanografeni numerose applicazioni con risultati promettenti [1]. Questa tesi si concentra sulla molecola di Dibenzo[hi,st]ovalene funzionalizzata con due gruppi mesitili e due atomi di cloro (DBOVMes-Cl). Lo studio si concentra sulle sue proprietà optoelettroniche e sull'interazione tra foto-eccitazione elettronica e gradi di libertà vibrazionali. Tale analisi è stata resa possibile da tecniche avanzate di spettroscopia ultra-rapida. La spettroscopia elettronica bidimensionale (2DES) emerge come un potente strumento spettroscopico a tempo risolto, offrendo un'elevata risoluzione temporale e frequenziale. La modellizzazione dell'esperimento e la sua simulazione sono state sviluppate contestualmente, consentendo congetture sull'origine e sul ruolo delle vibrazioni molecolari negli stati eccitati e fondamentali. Il modello a oscillatori browniano e il modello a displaced oscillators sono stati applicati contemporaneamente a un sistema a due livelli per simulare un set di dati 2DES. Le simulazioni sono state in grado di predire l'evoluzione dello spettro 2D e la dinamica del segnale in modo che le quantità fisiche rilevanti potessero essere dedotte dai parametri del modello. Inoltre, le evidenze presentate sostengono un maggiore coinvolgimento nei modi vibrazionali dello stato eccitato rispetto rispetto allo stato fondamentale. Ciò può avere profonde implicazioni in processi come il trasferimento di energia e cariche all'interno della molecola.

Parole chiave: nanografeni, spettroscopia electronica bi-dimensionale, accoppiamento vibronico, modello ad oscillatori Browniani

Contents

Introduction

Material science at the nano and molecular scale has witnessed significant advancements in the last decades, offering a myriad of opportunities to tail nanostructures for diverse applications. Nanographenes comes from the confinement of graphene within a few nanometers causing the electronic structure to have a finite band gap. The technological breakthrough is therefore related to the extraordinary optoelectronics properties, this master's thesis focuses on a particularly promising nanographene structure with optoelectronic properties suitable for lasing [1]. Nanographene derivatives have a strong vibrational-electronic (vibronic) coupling. Vibrational modes coupled to electronic states have been suggested to drive ultrafast radiationless decays in biological as well as synthetic molecular systems, so that understanding the nuclear and electronic degrees of freedom interplay is crucial to describe the photophysical properties of the molecule. Two-dimensional electron spectroscopy (2DES) emerges as a powerful time-resolved spectroscopical tool, offering high temporal and frequency resolution, which allows to provide real time tracking of energy/charge transfer processes real time, and to unveil the origin and role of molecular excited and ground state vibrations. An experimental data set of such complexity does need an interpretive model, and not only that: by simulating a replica of such a data set, the effectiveness of such interpretive model can be directly assessed comparing the two results. Despite the physics underneath the experiment being well accepted, reproducing the data-set through a model still presents unknowns, arbitrary choices and discoveries. A plethora of interpretative models have been developed, this thesis will be focus on two of them, namely the Brownian oscillator model, and the displaced oscillator model. Despite dealing with vibronic coupling, the models are both fully adiabatic and they will be presented in their most simplified version of a two or three levels system. The use of both model combined allowed a full simulation of real 2DES experiment contributing to extract new and insightful knowledge of the sample. The modeling and simulation have been therefore addressed contextually with the experiments. The 2D spectroscopy experiments presented have been performed during my training at the Politecnico di Milano ultrafast optics laboratories in the spring of 2023 by Phd. Mattia Russo and Phd. Rafael Muñoz-Mármol.

1 | Theoretical modeling tools:

Light-matter interaction studies represent one of the most successful and yet still innovative field of physics. In centuries all kind of models and formalism have been developed to describe quantitatively such interaction. This thesis resigns from any means of a comprehensive presentation, only the theoretical tools used in the following chapters, and relative to the 2DES experiments, are here presented as a compendium of several deeper and beautiful general treatments. To describe properties and temporal evolution of physical systems, a very general label that could apply at same time to atoms, electrons as to macroscopic experimental sample and to the electromagnetic field, needs first a mathematical representation of the systems. The physics of the systems is then hidden in the assumptions that lead to the formulation of equations. The success and validity of such description is then a matter of the use and experimental verification obtained by. To this extend different representation could be equivalent or, as in the following case, considered more favourable since more conveniently generalized to include different aspects. An example of it,the density operator description will be later favored in respect to the wave-functions. This new representation formalism works greatly also for the exact opposite case: which corresponds to find physical quantity's analytical expressions through a less general treatment of the problem where previously acquired knowledge can be thus conveyed. The interaction picture is a perfect example of it.

The system adopted in this thesis can be assumed as a single molecule that interacts with and electric magnetic field. The molecules form an ensemble where quantum coherences and classical uncertainty coexist and need to be addressed. The magnetic part of the E. M. field interaction is associated to a negligible energy and the remaining electric filed has low enough frequency and high enough intensity so that it is treated classically.

1.1. Classical mixture description: the density operator and Liouville Von Neumann equation

By considering a state $|\Psi\rangle$, the state is said to be a pure quantum state if its description presents no uncertainty beside the intrinsic quantum uncertainty. In this case, from $|\Psi\rangle$ a density operator, ρ, is defined as

$$\rho = |\Psi\rangle \langle\Psi| \tag{1.1}$$

The definition can be generalized to describe an ensemble of states in which an additional classical statistically distributed uncertainty is present. In the case of the molecular ensemble, the light-interaction could bring a single molecule in coherent superposition of ground and excited state, this condition represents a coherence state and it is the source of quantum uncertainty. (There nothing special about it, every quantum state describes a coherent super position of states in respect to some basis.) Actually not every molecule interacts with the field, some statistical reasoning can be brought to define a certain portion of molecules that did interact with the field whereas the remaining part did not. This bring the system in a classical, incoherent, superposition of states. ρ definition, eq. 1.1, can be thus generalized to comprehend such reality. In this case:

$$\rho = \sum_k P_k |\Psi_k\rangle \langle\Psi_k| \tag{1.2}$$

where $|\Psi_k\rangle$ expresses the different pure quantum states in the mixture and P_k is the classical probability for the system of being in it. The wavefunction formalism can not describe such classical mixture, therefore to study the time-evolution of the system a different formulation of the Schrodinger equation is needed. [2] The Liouville-Von Neumann equation addresses this need relating the time derivative of ρ to the Hamiltonian, H, of the system.

$$\frac{\partial}{\partial t}\rho = -\frac{i}{\hbar}(H\rho - H\rho) = -\frac{i}{\hbar}[H, \rho] \tag{1.3}$$

For an unperturbed Hamiltonian, this equation predict for each of the density matrix element a constant amplitude. However the coherence states are usually very short lived and rapidly decay $(10 - 100 fs)$ to a population state; the population states are described by the diagonal elements of ρ. A relaxation towards more stable states can be experimentally acknowledged to happen from excited states to the ground state.[3] The easiest way to account for this phenomena is adjusting equation 1.3 to include such behaviour, called dephasing for coherence states and relaxation for population states. The Liouville

representation let expressing it in a very compact way:

$$\frac{\partial}{\partial t}\rho = -\frac{i}{\hbar}L\rho - \Gamma\rho \tag{1.4}$$

where L stands for the operation $[H, ...]$ and Γ accounts for the exponential decay of coherence and excited states. Te Liouville equation 1.4 equation fully describes our system, the unperturbed case expression are trivially obtained and reflects phenomenological description. The next sections will focus on evaluate the time dependent Hamiltonian treatment to consider the interaction with an E.M. field.

1.2. Perturbed system: time dependent Hamiltonian

Including the radiation field inside the problem gives rise to a much greater complexity and thus a choice to face. The first option would mean to include the field's degree of freedom along the matter's one. This lead to a time-independent Hamiltonian with a much bigger phase space. Looking for solutions of the problem in such a large phase space turns out to be a too hard challenge. The second choice is to describe the radiation field as an external force, keeping only the matter's degree of freedom. Whereas time-dependent Hamiltonian follows as consequence of this second choice, new paths for advantageous simplification opens up, foremost the classical approximation of the field.

It is convenient to introduce here the ubiquitous tool of a time evolution operator, the following is a general definition of it:

$$|\Psi(t)\rangle \equiv U(t, t_0)\,|\Psi(t_0)\rangle \tag{1.5}$$

This operator allows to describe the time evolution in general, without the need of specify initial conditions. Without the use of the time evolution operator, the Schrodinger equation is to be solved any time the initial conditions are varied. With this said, time-dependent Hamiltonian are still a fair threat to treat exactly and the truncation of the consequently series expansion leads to very short holding approximations. The time evolution operator for the case of a time dependent Hamiltonian is given by following the time ordered expansion:

$$U(t, t_0) = 1 + \sum_{n=1}^{\infty}\left(-\frac{i}{\hbar}\right)^n \int_{t_0}^{t} d\tau_n \int_{t_0}^{\tau_n} d\tau_{n-1} \cdots \int_{t_0}^{\tau_2} d\tau_1 H(\tau_1)H(\tau_2)\ldots H(\tau_n) \tag{1.6}$$

Figure 1.1: Time variables of the time ordered expansion (Eq.1.6)

A change of system representation comes handy once more, the Interaction picture gives in fact a way to re-express the wave functions and their operators under a different point of view. The Hamiltonian is arbitrarily split in H_0, a simpler Hamiltonian which results in a time evolution operator that can be calculated exactly, and in $H'(t)$ more complicated that will be treated perturbatively. The partition choice has in principle no boundaries and choosing H_0 to be equal to zero, so that $H' = H$, the Schrodinger picture is obtained, whereas if the opposite choice is made the description of the system will follow the Heisenberg picture. Of course no measurable results is affected by the choice.

The Interaction picture offers very convenient solutions when the overall time dependent Hamiltonian can be partitioned in a greater and time independent H_0, describing the molecules' degree of freedom, and in a much weaker $H'(t)$ to include the interaction with the impinging electric field. In this case the time evolution operator of the non interacting system is simply given by:

$$U_0(t, t_0) = e^{-\frac{i}{\hbar}H_0(t-t_0} \tag{1.7}$$

whereas the weak perturbation in the interaction picture is given by:

$$H'_I(t) = U_0^\dagger(t, t_0)H'(t)U_0(t, t_0) = U_0^\dagger(t, t_0)(E(t) \cdot \mu)U_0(t, t_0) \tag{1.8}$$

with $E(t)$ being the impinging radiation field, and μ the dipole operator in the Schrodinger picture, once the dipole approximation is made. Switching from the Schrodinger to the Interaction picture through $U_0(t, t_0)$ does not eliminate the need for a series expansion to express operators. Despite that, the expansion is performed only to treat a weak perturbation and not the entire Hamiltonian. This makes the series expansion a powerful tool since truncating it at the n-th order gives a much more meaningful approximation. In this sense, the evolution of the density matrix $\rho(t)$ is written in series as:

$$\begin{aligned}\rho(t) = 1 + \sum_{n=1}^{\infty}\left(-\frac{i}{\hbar}\right)^n \int_{t_0}^{t} d\tau_n \int_{t_0}^{\tau_n} d\tau_{n-1} \cdots \int_{t_0}^{\tau_2} d\tau_1 E(\tau_n) \dots E(\tau_1) \\ \times U_0(t, t_0) \cdot [\mu_I(\tau_n)[\mu_I(\tau_{n-1}) \dots [\mu_I(\tau_1), \rho(-\infty)]] \dots] \cdot U_0^\dagger(t, t_0)\end{aligned} \tag{1.9}$$

Knowing to express the matrix density of a system is nothing less to what is required to

express the evolution of any physical observable. For a multi-dimensional spectroscopy experiment the objective observable is the non-linear macroscopic polarization.

The macroscopic polarization, P is defined as a classical optics quantity to describe the matter's response to an incident electric field. Without loosing generality, one can introduce a infinite set of susceptibilities tensor so that the polarization is often expressed as a power series of the electric field:

$$P = \epsilon_0(\chi^{(1)} \cdot E + \chi^{(2)} \cdot E \cdot E + \chi^{(3)} \cdot E \cdot E \cdot E + \dots \tag{1.10}$$

As a quantum quantity the macroscopic polarization is defined as the expectation value of the dipole operator μ. Bringing together the matrix density formalism and the Interaction formalism, one gets:

$$P(t) = \mathrm{E}[\mu] = Tr(\mu\rho(t)) \equiv \langle \mu\rho(t) \rangle \tag{1.11}$$

Some conventions are here introduced to uniform the notation with the rest of the work. When no radiation field is present, and right before it is, the system is assumed to be at equilibrium so t_0 can be brought back to $-\infty$, in this way one can set $\tau_1 = 0$ as an arbitrary and convenient choice for the time-zero point. Once the frame of reference is set, the time variables τ_n denote absolute time instants and new variables t_n are introduced to indicate the time intervals so that:

$$t_n = \tau_{n+1} - \tau_n \tag{1.12}$$

With some properties in mind, trace operator $\langle \dots \rangle$ is invariant to cyclic permutation and time evolution operator is unitary the n-th order Polarization is given by the use of $\rho(t)$ expansion (Eq.1.9) inside $P(t)$ definition (Eq.1.11):

$$\begin{aligned} P^{(n)}(t) = \int_0^\infty dt_n \int_0^\infty dt_{n-1} \cdots \int_0^\infty dt_1 E(t - t_n) E(t - t_n - t_{n-1}) \dots \\ \dots E(t - t_n - \dots - t_1) \cdot S^{(n)}(t_n, t_{n-1}, \dots, t_1) \end{aligned} \tag{1.13}$$

with S being the n-th order non linear response function of the system, defined as:

$$\begin{aligned} S^{(n)}(t_n, \dots, t_1) = \left(-\frac{i}{\hbar}\right)^n \langle \mu_I(t_n + \dots + t_1) \\ [\mu_I(t_{n-1} + \dots + t_1)) \dots [\mu_I(0), \rho(-\infty)] \dots] \rangle \end{aligned} \tag{1.14}$$

The response function, defined only for positive times t_n describes how the material behaves while interacting with an electric field. As it can be noticed only the first n dipole

operators are in the commutators while the last is not. As a matter of fact, n interactions with the field are present and they are represented by μ_I evaluated at the first n time instants $\tau_1 \dots \tau_n$, those interactions generate a non-equilibrium matrix $\rho^{(n)}$, whose off-diagonal elements at time $\tau_n + t_n$ emit a light field. The full derivation of the equations and more insights are present in literature and in particular in the works at [4] and [2].

1.3. Third-order response function:

To fully characterize the n-th order response function of a system, n interactions with the field are to be accounted for. In this case, explicitly writing the nested commutators in Eq.1.14, one obtains 2^n terms, each of them in pair with its conjugate complex for a total of 2^{n-1} independent terms. The number of terms increases even more when considering the multiplication with the electric field terms in the polarization expression, Eq.1.13). 2D spectroscopy, like most of the non-linear spectroscopy techniques, focuses on the third-order polarization term. Additionally, in media with spatial inversion symmetry even-order polarization terms vanish, therefore for most media the third-order term represents the lowest order non linearity. The third order overall response function, $S(t3, t2, t1)$, is thus obtained by a combination of 4 independent terms:

$$S^{(3)}(t_3, t_2, t_1) = \left(-\frac{i}{\hbar}\right)^3 \sum_{i=1}^{4} [R_i(t_3, t_2, t_1) - R_i^*(t_3, t_2, t_1)] \tag{1.15}$$

where:

$$R_1(t_3, t_2, t_1) = \langle \mu_I(t_1)\mu_I(t_1 + t_2)\mu_I(t_1 + t_2 + t_3)\mu_I(0)\rho(-\infty)\rangle \tag{1.16}$$

$$R_2(t_3, t_2, t_1) = \langle \mu_I(0)\mu_I(t_1 + t_2)\mu_I(t_1 + t_2 + t_3)\mu_I(t_1)\rho(-\infty)\rangle \tag{1.17}$$

$$R_3(t_3, t_2, t_1) = \langle \mu_I(0)\mu_I(t_1)\mu_I(t_1 + t_2 + t_3)\mu_I(t_1 + t_2)\rho(-\infty)\rangle \tag{1.18}$$

$$R_4(t_3, t_2, t_1) = \langle \mu_I(t_1 + t_2 + t_3)\mu_I(t_1 + t_2)\mu_I(t_1)\mu_I(0)\rho(-\infty)\rangle \tag{1.19}$$

The different terms can be seen as pathways of interaction and Liouville pathways and double-sided Feynman diagrams help to visualize and count all the possible interaction pathways. In this work only the Feynman diagrams will be showed but a more formal and complete treatment of both techniques is present at [5]. For the third order response the four independent terms are then expressed as the following diagrams:

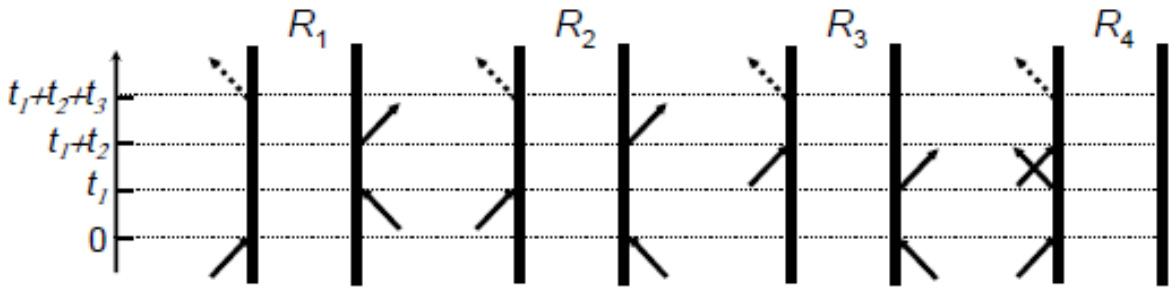

Figure 1.2: Double sided Feynman diagrams for the third order response function ([6])

From $S^{(3)}$, the third order macroscopic polarization field can be calculated accounting for the impinging electric field terms. In a 2D spectroscopy experiment, the electric field is composed by three pulses, this dramatically increases the number of terms but further approximations could reduce considerably the number of terms. Those approximations are here listed:

- Time Ordering
- Rotating Wave Approximation (RWA)
- Phase Matching

Straight forward experimental argumentation justify both RWA and the phase matching condition. The Time Ordering hypothesis need a more advance characterization and different experimental regimes can be found to not respect time ordering. As an example in a pump-probe experiment the first interactions are said to come from the same pump pulse breaking the time ordering symmetry. Nevertheless throughout all the simulations Time Ordering hypothesis holds as true for every t_1, t_2, t_3. To enforce so, the semi-impulsive limit is applied and the total electric field is written as:

$$E(t) = [E_1\delta(t) + E_2\delta(t-\tau) + E_3\delta(t-\tau-T)][e^{i\omega t - k\cdot r} + e^{-i\omega t + k\cdot r}] for t, \tau, T \geq 0 \quad (1.20)$$

The macroscopic polarization is then simply given by:

$$P^{(3)}(t) = S^{(3)}(t, \tau, T) \quad (1.21)$$

The discussion can be then fully translate to the characterization of the response functions R_i.

1.4. Semi-classical simulation and response function equations:

Finding analytical expression to be able to simulate the response functions of a complex systems can be tricky and even impossible. Equations from 1.16 to 1.19 are still implicit, and thus general, expressions, and they are not yet useful for simulations. The system should be then characterized as number of involved levels, coupling terms in the Hamiltonian and phenomenological parameters. The most simple cases are the two or three energy level systems non interacting and with pure phenomenological parameters to characterize the response function from the experimental data. Such equations will be presented in the third chapter while discussing a specific simulation model. In this section, two different Hamiltonian models for a two level system are presented in order to address from more first principle considerations, the complexity of the experimental response function. As it will be shown in the third chapter, not only changing the Hamiltonian could help for a deeper data analysis, but it let the simulated response function to predict and quantify data phenomena, otherwise only describable subsequently the experiment. Out of all the possible features that a 2D spectroscopy data set can show, the following Hamiltonian model addresses two main phenomena: the lineshape evolution along t_2, in terms of spectral diffusion and the stokes shift, and the oscillation dynamics that $S(t_1, t_2, t_3)$ sometimes show again along the t_2 axis. Both models comes from a fully adiabatic treatment and the Condon principle is used to simplify the overall problem.

1.4.1. The Brownian oscillator model: a microscopic theory of dephasing

Stochastic processes are commonly used in the modeling of complicated system's response function. A stochastic model, in this case, allows to derive an overall response function that, accounting for the dephasing of the electronic coherence and for a common and random environment interaction, predicts the response function to evolve showing the spectral diffusion and the stokes shift. The molecule is, in fact, assumed to be in a bath that exerting random forces on the molecule makes the electronic energy gap a stochastic process itself. This makes the matter's Hamiltonian, now referred as H_s, time-dependent too. To account for it, one can introduce the energy gap operator, Ω, defined as:

$$\Omega \equiv H_1 - H_0 - (\epsilon_1 - \epsilon_0) \tag{1.22}$$

Where $H_1 = \langle 1| H_s |1\rangle$, $H_0 \langle 0| H_s |0\rangle$ are the eigenvalues of the two level electronic problem in the bath and ϵ_1, ϵ_0 are their relative in the isolated, thus deterministic, case. Then the off-diagonals dipole operator matrix element are expressed as:

$$\mu_{01}(t) = \mu e^{-\frac{i}{\hbar}(\epsilon_1-\epsilon_0)t} exp_+(-\frac{i}{\hbar}\int_0^t \Omega(\tau)d\tau) \tag{1.23}$$

$$\mu_{10}(t) = \mu e^{-\frac{i}{\hbar}(\epsilon_1-\epsilon_0)t} exp_-(\frac{i}{\hbar}\int_0^t \Omega(\tau)d\tau) \tag{1.24}$$

where exp_+ and exp_- compactly express the time order expansion as in the equation 1.6. Once put in the general expression of the response functions (eq. 1.16 to 1.19) a cumulant expansion to the second order of the stochastic process described by $\Omega(t)$ can be done to obtain the expression of the lineshape function g(t):

$$g(t) = \frac{1}{\hbar^2}\int_0^t d\tau \int_0^\tau d\tau' \langle \Omega(\tau)\Omega(\tau')\rho(-\infty)\rangle \qquad with \quad \tau \geq \tau' \tag{1.25}$$

Expanding a distribution up to its second cumulant is of common use to simplify expected values computation of complicated expression. It is indeed a powerful tool, especially if $\Omega(t)$ is a Gaussian process in that case the expansion would be formally exact. To $g(t)$ is possible to refer the explicit response functions equations:

$$R_1(t_1,t_2,t_3) = (\frac{i}{\hbar})^3 \mu^4 e^{-\frac{i}{\hbar}(\epsilon_1-\epsilon_0)(t_1+t_3)} exp(-g(t_1) - g^*(t_3) - f_+(t_1,t_2,t_3)) \tag{1.26}$$

$$R_2(t_1,t_2,t_3) = (\frac{i}{\hbar})^3 \mu^4 e^{-\frac{i}{\hbar}(\epsilon_1-\epsilon_0)(t_1-t_3)} exp(-g^*(t_1) - g^*(t_3) + f_+^*(t_1,t_2,t_3)) \tag{1.27}$$

$$R_3(t_1,t_2,t_3) = (\frac{i}{\hbar})^3 \mu^4 e^{-\frac{i}{\hbar}(\epsilon_1-\epsilon_0)(t_1-t_3)} exp(-g^*(t_1) - g(t_3) + f_-^*(t_1,t_2,t_3)) \tag{1.28}$$

$$R_4(t_1,t_2,t_3) = (\frac{i}{\hbar})^3 \mu^4 e^{-\frac{i}{\hbar}(\epsilon_1-\epsilon_0)(t_1+t_3)} exp(-g(t_1) - g(t_3) - f_-(t_1,t_2,t_3)) \tag{1.29}$$

$$\begin{aligned} where: f_-(t_1,t_2,t_3) &= g(t_2) - g(t_1+t_2) - g(t_2+t_3) + g(t_1+t_2+t_3) \\ f_+(t_1,t_2,t_3) &= g^*(t_2) - g(t_1+t_2) - g^*(t_2+t_3) + g(t_1+t_2+t_3) \end{aligned} \tag{1.30}$$

The line shape function $g(t)$ is in general a complex function, therefore R_1, R_4 and R_2, R_3 are no longer equal. The Brownian oscillator is thus able to distinguish from excited state responses, R_2 and R_4, and ground state ones, the remaining R_1 and R_3 . This distinction can be crucial to characterize sample's behavior in respect to determined phenomena. Before getting a full explicit response functions, some characterizations are needed on

$g(t)$, the time ordered integral of the correlation function:

$$C(t) = \frac{1}{\hbar^2}\langle\Omega(\tau)\Omega(\tau')\rho(-\infty)\rangle \tag{1.31}$$

As a correlation function of Hermitian operators, $C(t)$ complies with many symmetry properties both in the time domain and in its frequency representation. In the frequency domain, an important result of such properties is represented by the very general fluctuation-dissipation theorem:

$$Re[\tilde{C}(\omega)] = coth(\beta\hbar\omega/2)Im[\tilde{C}(\omega)] \tag{1.32}$$

Leaving the full derivation to the reference at [7], for the case of a continuous distribution overdamped Brownian oscillators in the high temperature limit, g(t) assumes the form given by:

$$\begin{aligned} g(t) = &\frac{2\lambda k_B T\tau_C^2}{\hbar}[exp(-t/\tau_C) + t/\tau_C - 1] \\ &- i\lambda\tau_C[exp(-t/\tau_C) + t/\tau_C - 1] \qquad k_B T >> \hbar\Lambda \end{aligned} \tag{1.33}$$

A deep characterization of each parameter is shown later in the first part of the third chapter. For now, new emphasis is given to the physics behind the model. The expression of $g(t)$ is in deed fairly general and it could see disparate kinds of application. Here it is used to described the coupling of the molecule with a phonon bath made of a continuum of Brownian oscillators, so with an inherited stochastic nature. In this sense the optical response can be characterized in many ways and the original phenomenological dephasing case is retrieved as limiting case of such expression.

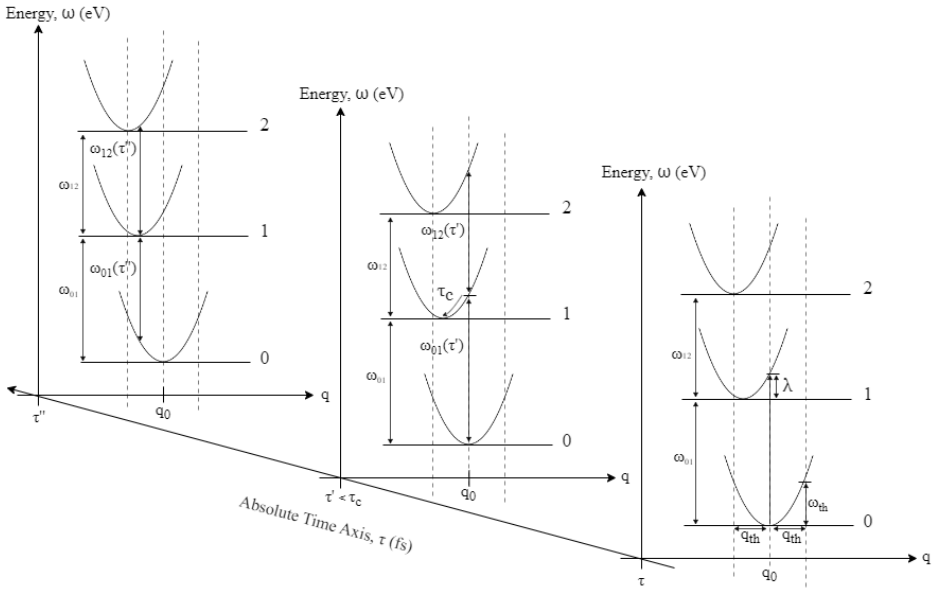

Figure 1.3: A pictorial visualization of the Brownian oscillator model, the physical meaning of the $g(t)$ parameters τ_C and λ is qualitatively explained

In addition to the literature of reference [8], a weak generalization to a three level system has been developed in order describe a third kind of optical signal typical of a 2D spectra. Even though in a two level system only two kind of contributions, and both positive, are possible, for more articulated systems 2D spectroscopy signals could show a negative, and generally spread, contributions. Two new response functions are then derived:

$$\begin{aligned} R_5(t_1,t_2,t_3) = &-(\frac{i}{\hbar})^2\mu^4 e^{-\frac{i}{\hbar}((\epsilon_2-\epsilon_1)t_3-(\epsilon_1-\epsilon_0)t_1)} \\ &exp(-g^*(t_1)-g(t_3)+f_-(t_1,t_2,t_3)) \end{aligned} \tag{1.34}$$

$$\begin{aligned} R_6(t_1,t_2,t_3) = &-(\frac{i}{\hbar})^2\mu^4 e^{-\frac{i}{\hbar}((\epsilon_2-\epsilon_1)t_3+(\epsilon_1-\epsilon_0)t_1)} \\ &exp(-g(t_1)-g(t_3)-f_-^*(t_1,t_2,t_3)) \end{aligned} \tag{1.35}$$

where f_- and f_+ are given at equation 1.30. For simplicity all the parameters of the third level, but the energy gap, were kept equal to the ones describing the first two. In total six independent response functions have been defined so far, R_1, R_2, R_3, R_4, R_5, R_6. R_2 and R_1 give, respectively, the rephasing and the non rephasing stimulated emission contribution. R_3 and R_4, the rephasing and the non rephasing ground state bleaching (or photo bleaching) contribution. R_5 and R_6, the rephasing and the non rephasing excited state (or photo induced absorption). Here a pictorial image of the three kinds of 2D spectroscopy signal:

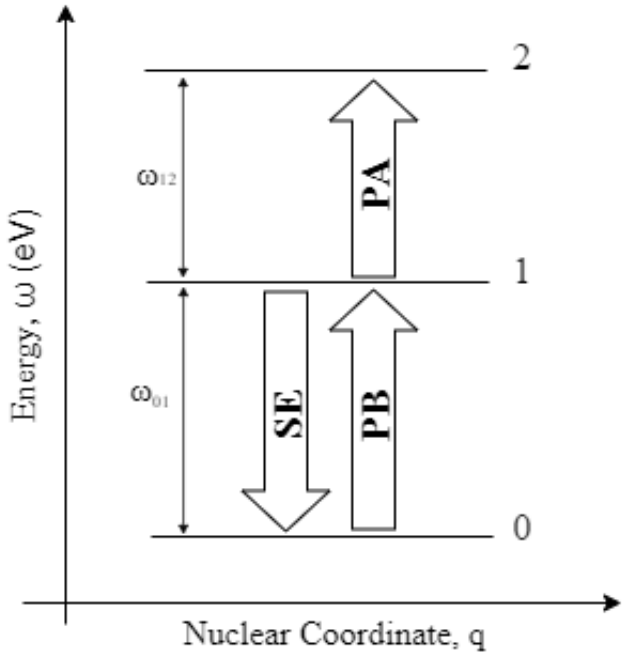

Figure 1.4: Three contributions can be found. Here they are explained in the most simple, but comprehensive model. SE stands for stimulated emission, PB for photo bleaching and PA for photo induced absorption

1.4.2. Vibrational dynamics and the displaced oscillator model

The presentation of the next model works as a theoretical introduction for a more deep discussion, strong of the simulation results, present in the second half of the third chapter. The objective of introducing such model is to describe vibrational dynamics that multi dimensional experiments show in the transient absorption (or transmission) spectra. The model is again fully adiabatic, thus it does not include non adiabatic effects as coherent mixing of electronic and vibrational degrees of freedom. The model is presented as in the following figure in its simplest formulation, namely the one of a two level system with a single vibrational mode and at the zero-temperature limit.

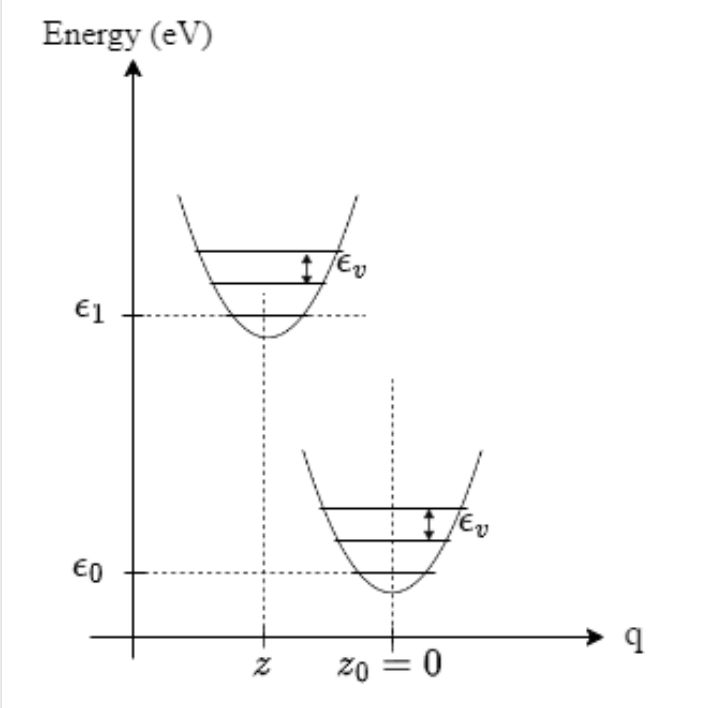

Figure 1.5: Pictorial representation of the displaced harmonic oscillator model. The q-axis represent the quadrature $X = \frac{1}{2}\langle a^\dagger + a\rangle$. The parameters energies ϵ and the displacement z are the one entering the Hamiltonian in eq. 1.36

The model exploits the coherent states formalism to treat the vibrational degree of freedom with simplicity without any loss of generality. The Hamiltonian's model reads:

$$\begin{aligned} H = &|0\rangle\langle 0|\,(\epsilon_0 + \epsilon_v(a^\dagger a) \\ &+ |1\rangle\langle 1|\,(\epsilon_1 + \epsilon_v(a^\dagger + z)(a + z) \end{aligned} \tag{1.36}$$

The vibrational part of Hamiltonian depends in fact on the electronic eigenstates, but only on the displacement parameter z. This keeps the two kind of variables separated so that each R_i response function can be written as a product of the electronic response function and of the vibrational one:

$$\forall i = 1, .., 4 \qquad R_i = R_i^{(e)} R_i^{(v)} \tag{1.37}$$

The full derivation of the the third order response functions can be found in the article at reference [9]. In the following the consequently derived vibrational response function are listed:

$$\begin{aligned} R_1^{(v)} = &exp[z^2(-2 + e^{-i\Lambda_{111}} + e^{i\Lambda_{010}} + e^{i\Lambda_{001}} \\ &+ e^{-i\Lambda_{100}} - e^{i\Lambda_{011}} - e^{-i\Lambda_{110}})] \end{aligned} \tag{1.38}$$

$$R_2^{(v)} = exp[z^2(-2 + e^{i\Lambda_{110}} + e^{-i\Lambda_{011}} + e^{i\Lambda_{001}} - e^{-i\Lambda_{010}} + e^{i\Lambda_{100}} - e^{i\Lambda_{111}})] \tag{1.39}$$

$$R_3^{(v)} = exp[z^2(-2 + e^{i\Lambda_{100}} + e^{-i\Lambda_{001}} - e^{i\Lambda_{010}} + e^{i\Lambda_{011}} + e^{i\Lambda_{110}} - e^{i\Lambda_{111}})] \tag{1.40}$$

$$R_4^{(v)} = exp[z^2(-2 + e^{-i\Lambda_{100}} + e^{-i\Lambda_{001}} + e^{-i\Lambda_{010}} - e^{-i\Lambda_{011}} - e^{-i\Lambda_{110}} + e^{-i\Lambda_{111}})] \tag{1.41}$$

where:

$$\Lambda_{p_1,p_2,p_3} \equiv \frac{\epsilon_v}{\hbar}(p_1 t_1 + p_2 t_2 + p_3 t_3) \tag{1.42}$$

Despite many kind of generalization can be proposed from these results, two are crucial to simulate such vibrating system: 1-Finite temperature case, 2-Vibrational relaxation. The most simple to obtain is the finite temperature case. In the zero-temperature case the system was always initialized in the ground state of the undisplaced oscillator, whereas the presence of a finite temperature imposes the initial state to an arbitrary $\langle \alpha_0 |$ state. Forming the coherent states a complete basis of the phase space, such state can always be expressed as combination of coherent states. In this way, deriving the effect of such initialization leads to really the same response functions only multiplied by a scalar factor equal, in the high temperature limit, $\frac{2k_B T}{\epsilon_v}$. The second generalization aims to include the experimental evidence of a vibrational dump in the oscillating dynamics of the response functions. Despite being conceptually simpler than the finite temperature arbitrary initialization, its implementation requires quite tedious calculation that are fully reported on a article by F.Troiani and colleagues [9]. The crucial change is summarized by the next relation:

$$\epsilon_v -> \epsilon_v + i\frac{\hbar}{\tau_v} \tag{1.43}$$

The once real parameter ϵ_v become a complex affecting the Λ_{p_1,p_2,p_3} operator and introducing a prefactor given by:

$$f(t,\alpha) = exp[-\frac{|\alpha + z_k|^2}{2}(1 - e^{-t/\tau_v})] \tag{1.44}$$

The new parameter τ_v is then introduced in the simulation model and in the third chapter the resulting response functions are then fully characterized by each individual parameter.

2 | Experiments and simulation methods:

"What we cannot learn with 2D spectroscopy we will not be able to learn with any other third order spectroscopy" Peter Hamm in his "Principles of Nonlinear Optical Spectroscopy: A Practical Approach"[10]

Third order non linear spectroscopy is a fertile and vital experimental physics field. Many different examples of experiment and application can be made. In this chapter the two-dimensional electronic spectroscopy (2DES) is presented in its experimental implementation. 2DES is a powerful ultrafast spectroscopy technique that provides detailed information about the electronic energy states and dynamics of molecules in condensed-phase systems. The investigated spectrum region is thus the visible spectrum. 2DES set up employs a sequence of three ultrashort laser pulses to excite and probe the sample. The first two pulses that interact with the sample act as a pump and they are responsible of initiating the excitation process and causing an out of equilibrium condition in the system density matrix. The third pulse, instead, is called probe and it used to monitoring, or 'probing', the system relaxation back to an equilibrium condition. The three pulses define two time intervals, namely t_1 and t_2. The latter is also called "waiting time" or "population time". This chapter focuses on the description of the experimental apparatus adopted in this thesis and the simulation architecture to extract information from the measurements.

2.1. Experimental setup:

2D spectroscopy combines high temporal and spectral resolution by providing a perfect tool to study ultra fast dynamics in complex system. This is possible thanks to the multiple and time ordered interaction that the sample experience with the electromagnetic field. In fact, other transient spectroscopy experiment faces a restrictive compromise between temporal and resolution, given by the duration of the pulses, and a frequency resolution, given by the bandwidth of the pulse. In a Pump-probe experiment for example, one of

the most common third-order spectroscopy experiment, the pump frequency resolution in the excitation spectrum is simply given by the width of the pump pulse spectrum [11]. In two pulses experiment the two resolutions form a duality: if the pump pulse lasts few optical cycles, giving high temporal resolution, its spectrum will be very broad with no information on the excitation frequency; the opposite is true for long, and thus narrow band, pulse. The use of a third pulse in a 2D spectroscopy set up disentangles such duality. The frequency resolution it is in fact related to the temporal resolution and the tunability of the delay, namely t_1, between the two pump pulses. The probe pulse then interferes with the out of equilibrium sample and it is delayed with respect the second pump pulse by the delay t_2. The emitted signal is then scattered in different directions each given in compliance with the phase-matching condition. A detector is then generally placed along the direction where the signal under investigation is expected to propagate. Such preferred direction depends on geometry of the pulses and on the kind of signal to be analyzed [12]. The sample response propagates along the time interval called t_3 and typically interacts with a fourth pulse that works as 'local oscillator' and gives the interferometric measure as a function of t_1, t_2, t_3. The signal is then visualized, by means of the Fourier transform, as function of ω_1, ω_3, the excitation frequency and detection frequency respectively, and t_2. Therefore the signal gives a correlation map between excitation and detection frequency recorded for several t_2 instants, potentially elucidating the mechanisms of ultra fast energy and charge transfer in systems like photosynthetic light-harvesting complexes, molecular crystals, and semiconductors. Out of the possible signals visible in a 2D map, two family can be distinguished: the diagonal peaks, that correspond to the linear spectrum and whose shape gives information on the homo/inhomogeneous broadening and on all the characteristics derived from the broadening; the cross peaks out of the diagonal which instead show couplings between the excitation states electronic and vibrational [13]. The excitation signal can be thus characterized by frequencies, intensity, shape and time evolution allowing a quantification of excited states couplings and real time description pathways of energy/charge flow from one state to the other [13, 14].

All of these possibilities and resolution power come with technical difficulties and experimental challenges. Those challenges depend of the spectrum region of the employed light, in the 2DES case the explored spectrum region overlaps with the visible spectrum of light. Higher or lower energy 2D spectroscopy experiments are possible and they all present some similar and yet unique challenges. 2DIR, a 2D spectra measurement in the infrared region, is a well explored technique to probe and characterized molecular vibrational states, their coupling and energy transfer processes [15]. To be able to collect meaningful 2D signal, an interferometric stability between pairs of excitation pulses is required to be below fraction

of their carrier wavelengths. To this extent the control of the pump pulses relative phase stability is an easier challenge at lower energy, like the 2DIR case. Nevertheless there are different experimental techniques that offer the required phase stability.

In the ultrafast laboratory of Politecnico di Milano, where the presented work has been developed, the interferometric stability is reached by employing a translating wedge based identical pulses encoding system (TWINS) [16, 17] that allows to control the delay between the first and the second pulse with very high precision. The experimental apparatus adopted in the laboratory used the so called pump probe geometry configuration. This geometry configuration is also called "Collinear self-heterodyne 2D spectroscopy" [12], namely the pump pulses run in a collinear configuration and the detector is placed along the probe direction to comply with the phase matching condition. Here, ω_3 spectrum is retrieved directly from the emitted field thanks to a spectrometer. As mention before, different choices are still viable solutions having for each solution advantages and consequences in terms of stability, power of resolving different signals and acquisition time for a measure. A collinear geometry for the pump makes indistinguishable the rephasing and the non rephasing parts of the response function, as matter in fact in this case complying the phase matching condition locks both contribution along one direction, parallel to the probe wave vector. Therefore this configuration reduces considerably the complexity of the detecting apparatus and possibly halving down the acquisition time. In this way the measured signal corresponds to the, so called, Pure Absorptive spectra allowing a direct physical interpretation of the experimental results. This technique, despite the advantages, does not allow for background signals to get inside the detector, since it is placed along the probe propagating direction and needed artificially taken care either before or after the signal acquisition.

The generation of ultra short pulses with some frequency tunability represents the next challenge to face in order to accomplish a working 2DES experiment set up. To address a lower complexity in the set up, the three pulses are identical and the steps described in this paragraph to generate, tune and compress the pulses are shared among the three. It follows a brief explanation of the pulse generation segment. The setup uses a Ti:Sapphire laser in mode locking regime that emits 150 fs laser pulses whose spectrum is centered at $\lambda = 800nm$ and with 1 kHz repetition rate. Those pulses are then used to pump a non collinear optical parametric amplifier (NOPA) [18] to generate visible laser pulses with, in our case, a spectrum spanning from 550nm to 750nm. The pulse envelope is then temporally compressed with a pair of chirped mirrors through which the beam computes 7 bounces to reach a temporal duration below 20 fs [19]. The pump and the probe laser pulses for the 2DES experiment are then retrieved by separating the main beam by a non

symmetric beams splitter.

Acquiring 2DES data is not a straightforward activity, once having aligned and having put at work the setup, two main steps have to be checked before start. The first stadium combines the calibration of the pump pulses through an additional photo-diode giving the pump auto-correlation function along the t_1 axis. With this information is possible to retrieve empirically the best fit for the linear transformation between the "Pseudo Frequency" axis to the pump "Optical Frequency" axis. The psedudo-frequency axis is given by the Fourier transform of the t_1 axis sampled with mechanical steps of the delay stage, while the latter serves as excitation axis for the 2D spectra data [15, 20]. The second preliminary activity aim to asses the temporal duration of the pump and thus the experiment temporal and excitation frequency resolution. Temporal characterization of the pulses, whose duration is more than ten order of magnitudes shorter the camera and the electronics reading time, could be perform with different techniques. For this experimental set up, a "Polarization Gating Frequency-Resolved Optical Gating" (PG-FROG) measurement was implemented. The measure exploits a non-linear crystal whose refractive index depends on the intensity of the impinging beam. To ensure a meaningful result the crystal employed should be chosen upon the characteristics of the experiment's sample, in particular in respect to the length of beam's path inside the materials. For a sample in solution, like the case presented here, this requirement applies the the path length of the cuvette [11, 20].

Once the preliminary characterization have been terminated the setup could be use to acquire sample's data. As good practice for the first measurement is to scan the pumps-probe t_2 delay with $t_1 = 0$. Such measures coincides with the integration along the excitation axis of the 2D spectra and so to a broad band Pump-probe measure with only two pulses. Comparing a previously acquired 1D transient spectrum with the one obtained indicates a reliable sign of the validity of the next 2DES experiment, furthermore it gives a very high temporal resolution ($< 20fs$) pump probe measurement. The actual 2D spectroscopy proceeds scanning along the t_1 axis, in this case between $-30fs$ and $250fs$, for a fixed t_2 delay. Fourier transform can be then applied along the acquisition axis and the 2D spectra map is acquired. The next t_2 delay can be investigated, and so on iteratively to eventually obtain the full signal $S(\omega_1, t_2, \omega_3)$.

2.2. Simulation methodology compendium:

The simulation environment simplifies much of such complexity, but it still presents some challenges. The code, running the simulation, has been developed from scratch in python

programming language within the free-licensed "Spyder IDE" [21]. The simulation being fully deterministic, no random draws are present in the scripts, gives consistent results so that a modularity approach could be implemented. The program has been indeed divided in two parts: the first part generates the data whereas the second part implements the data analysis and visualization. The generation of the 2D data relies on the explicit expression of the response functions presented in the first chapter. The signal is thus generated in its time-domain to be later being transformed, via an FFT algorithm, to a frequency representation in respect of t_1 and t_3 axis. Beside choosing the model to be simulated and its relative system parameters, the user defines here some quantities to effectively run the simulation. Because of the Fourier transformation applied between the signals definition and their final representation it is crucial to carefully chose the time axis parameters. In particular for every time axis its span and the number of samples are to be defined considering the frequency span to be described and the frequency resolution that it is to achieved. This matches up the experimental restriction on time and frequency resolution, and likewise the simulation time grows when high number of points are taken. For every simulations and run model the same time axis have been defined. As a convention times are gonna be expressed in femtoseconds, where $1fs = 10^{-15}s$, and the its Fourier dual axis expressed in energy units of electron Volt (eV). For the t_1 and t_3 axis the simulation have been running up to $1ps$ with 1024 sampling points. In this way signals are resolved up to $2.11338eV$ with intrinsic spacing of $0.00413eV$. For t_2 axis the same span of $1ps$ has been chosen while a smaller number points were acquired, namely 512 points. Along the transformed t_2 axis, components with energies up to $1.005457eV$ are resolved with a spacing of $0.00412eV$ between points. This limits are well above the t_2 experimental energy resolution as it will be show in the fourth chapter.

The second part of the simulating program has been written on a different file and it could be run independently. Lasting the generation of data much more than the analysis, this turned to be crucial so that a great amount of data could be generated night long and the analysis could be performed at will of the scientist with a much quicker results. Different visualization protocols have been implemented within this algorithm, the most common two are: the 2D spectra for fixed t_2 referred as 2D map and the t_2 dynamics plot where ω_1 and ω_3 where fixed, usually on the signal peaks. A third way to visualize the full spectrum is referred in the text as pump-probe like representation. In this case the signal $S(\omega_1, t_2, \omega_3)$ is integrated along ω_1 and the obtained two variables function can be plot all in one scatter plot resembling a 1D pump probe map.

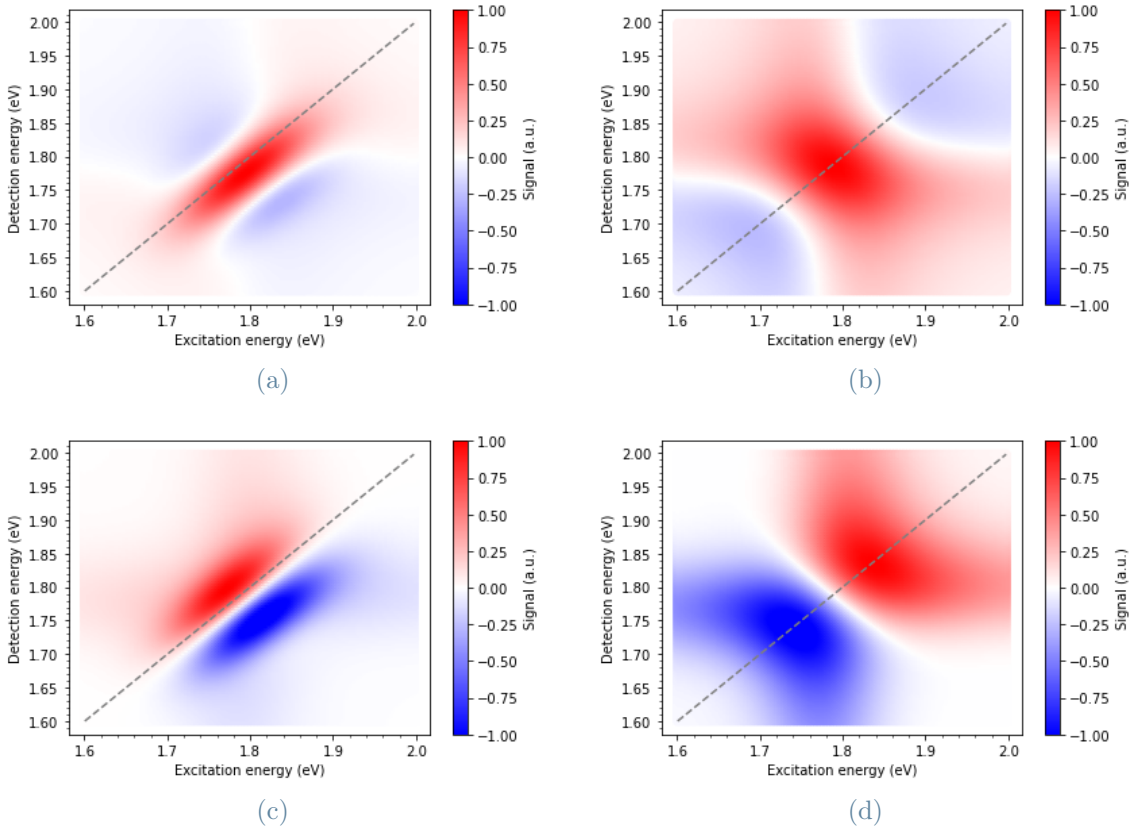

Figure 2.1: (a)Rephasing real part (b)Non rephasing real part (c)Rephasing imaginary part (d)Non rephasing imaginary part. Rephasing and non rephasing contributions can be individually generated in the simulation. Due to the pump-probe geometry, this is not possible experimentally.

2.2.1. From rephasing and non rephasing contributions to the pure absorptive spectrum:

As introduced in the first chapter one can partition the response functions in rephasing and non rephasing contributions. This division, despite coming purely from the density matrix formalism, hides a profound physical meaning. Two pulse photon echo effect can be experimentally shown and 2D spectroscopy experiments can be designed to acquires only one of the two kind of contribution. From the last section, the simulation is acknowledged to generate data individually from each response function R_i, how are they then combined to give an unique transient 2D spectra comparable to the one coming out from an experiment?

As an example of the difference of the two kind of contributions in figure 2.1 are shown the real and the complex part of the two kind of signals. For each map a deep characterization can be addressed, and this can be done also experimentally with 2D spectroscopy set up in a box geometry. In such geometry configuration of the pulses where the phase matching condition lets divide spatially the contribution. Nevertheless in the simulation only the pure absorptive signal is conserved and further analyzed. This follows a common convention to visualize in one 2D spectroscopy map both contribution [6] and it is consistent with the kind of data acquired by the experimental set up [16]. In the following equation the definition of the pure absorptive signal is given:

$$R_{abs} = \Re[R_{rephasing} + R_{nonrephasing}] \tag{2.1}$$

The purely absorptive spectrum preserves the sign of each contribution and sacrifices information on the dispersive contributions to a more compact and intelligible representation. Differently from other configurations, like box-car geometry, the pump probe configuration used in experimental set up combines with a special phase matching condition the two contributions so that spectrometer measures in single shot the pure absorptive spectrum.

3 | Model analysis:

3.1. System modeling and static description:

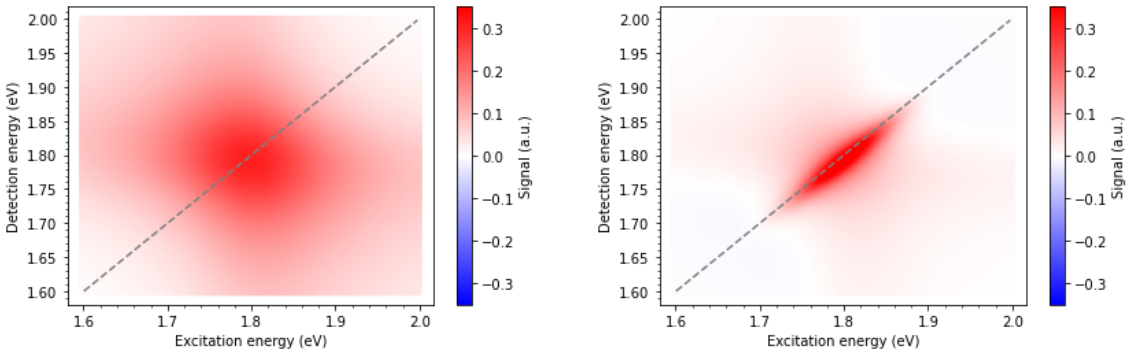

(a) (b)

Figure 3.1: (a)Homogeneous case, the isotropic Lorentzian broadening is dominant in the lineshape. (b)Inhomogeneous case, a Gaussian broadening along the diagonal dominates the lineshape

The simplest model for the simulations presented in this chapter is an isolated two level system. It often works as an initial benchmark to understand multi-dimensional spectroscopy data but it works finely when studying optical transitions in isolated monomer [12]. Therefore a unique parameter characterizes the model: eV01 (eV). The value of it coincides with the energy gap within the levels. The impulse response function of this simple system would be an impulse itself, this is nonphysical and the model should be already modified. To reproduce any measured spectrum, one has to introduce an uncertainty factor or broadening parameter. Being a multi interactions spectrum, such uncertainty should be modeled to account the excitation and the detection energy. The nature of such broadening can be various, an utmost fundamental reason can be retrieved to the quantum nature of the physical system and of it the energy states. Having the interaction a finite duration in time, the Heisenberg principle implies that some uncertainty in the energy has to expected and it cannot be lowered arbitrarily. For a 1 picosecond lasting experiment, with only the Heisenberg picture theory predicts an energy uncertainty of

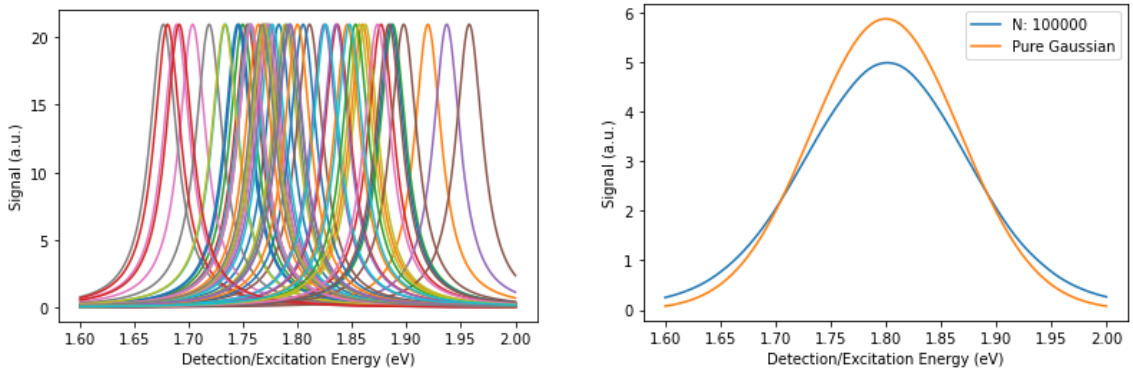

(a) (b)

Figure 3.2: An intuitive way to understand the building of a lineshape is thinking it as sum of Lorentzian distributions all characterized by a unique γ, each representing a molecule, whose centers is distributed as $\sim N(E01, \sigma)$. When the molecules are many, but still independent, the result diagonal profile resembles $\sim N(E01, \sigma)$ and the anti diagonal profile a Lorentzian $\sim L(E01, \gamma)$. (In the figure $\gamma = 0.01eV, \sigma = 0.04$)

roughly 10^{-23} Joules or 10^{-4} electron Volts. A commonly measured broadening exceeds such uncertainty by orders of magnitudes, therefore others and more empirical reasoning have to be introduced. As a general knowledge a light interacting molecule undergoes different dynamics and stochastic process can be adopted to account for the broadening of its absorption and emission spectrum. As a first approximation two families of broadening can be distinguished. A stochastic process of the first kind contributes to the so called homogeneous broadening and in frequency it generally follows a Lorentzian distribution shape. One of the second group causes a so called inhomogeneous broadening contributing to a more Gaussian distribution lineshape. Both of these processes can be described by a characteristic correlation timescale. When those are well separated, the ratio of the timescales is either big or close to zero, an independent treatment is formally correct and a simple convolution of the two distribution reproduces the results. Assuming so can very useful for all kinds of systems, but sometimes those timescales are indeed comparable. The stochastic processes can not be treated independently and all sorts of phenomena show up, introducing the need of a more complex formalism. For now, the discussion will only regard the first scenario: both kind of processes are present but the correlation timescales are uncoupled and so the resultant spectrum profile is given by a convolution of both contributions. The new lineshape would then follows what is said to be the Voigt distribution. To introduce a physical meaning to the discussion two physical assumptions of the model are to be introduced:

- Every molecule has a characteristic dephasing time constant after which the correla-

tion between the eigenstates is loss so that the non linear polarization signal would also fade to zero. Such time constant is equal for every molecule of the sample and it doesn't depend on the environment. It in fact accounts for the homogeneous Lorentzian-like broadening.

- The energy gap between the molecule's excited states depends on the many interactions with a non deterministic evolving environment. For simplicity, and strong of the Central Limit theorem, the resultant interaction it assumed to follow the Normal distribution centered in zero and described by the standard deviationσ.

Strong of these assumptions, several interesting aspects of system can be simulated and in the appropriate representation framework the simulation reproduces an experimental 2D spectral map. In the time domain out of the four response functions introduced in equations from 1.16 to 1.19 in their general expression the following two can be found:

$$R_3 = R_2 = R_{nonRephasing}(t1, t3) = A_{0NR} e^{-i\omega_{01}(t_3+t_1)} e^{-\gamma(t_3+t_1)} e^{-\sigma^2(t_3+t_1)^2/2} \tag{3.1}$$

$$R_1 = R_4 = R_{Rephasing}(t1, t3) = A_{0R} e^{-i\omega_{01}(t_3-t_1)} e^{-\gamma(t_3+t_1)} e^{-\sigma^2(t_3-t_1)^2/2} \tag{3.2}$$

As can be seen no distinction can be done between photo bleaching and stimulated emission signals. Following the assumptions, the newly introduced equations have introduced two new parameters to characterize the model:

- γ, the electronic states dephasing time constant, controlling the Lorentzian distribution width.
- σ, the standard deviation of molecule-environment interaction process.

In Figure 3.1 two different examples of map simulated in this way are given. Figure 3.1a shows the 2D map of a system with a lineshape dominated by its homogeneous broadening, as in figure 3.1b the opposite holds. The inhomogeneous gives the strongest contribution, but the changes in the lineshape are more dramatic than only the difference that insists between a Lorentzian distribution and a Gaussian curve. As it resembles in the second case, the lineshape is more elliptical, with a clear preferred direction in elongation along the diagonal x = y. Cutting the map along the main diagonal direction and its perpendicular, one could extract two different broadening profiles. Such profiles resemble the two bell shapes as distinguished as they were in the model assumptions. The reason why those directions are so special and whether the extracted distribution are respectively Gaussian and Lorentzian curves it will be here phenomenological explained. The non-trivial interpretation applied here is that the x and y axis represent the detection,

or emission, energy axis and the excitation energy axis. 3.1a shows the case of an isolated oscillator that strictly follows assumption 1 having the characteristic star-like shape [15]. It tells us that the two cut profiles are simple Lorentzian distribution centered in the energy gap of the states, eV01, and with a "full width at half maximum" (FWHM) controlled by the γ parameter. Such oscillator is now let to interact with a bath that randomly modifies its resonant frequency, form assumption 2, and this process independently to the thousands of sample's molecule in the solution and so it is replicated many many times in the simulation to model the sample the solution. The interacting light is now absorbed and emitted at each oscillator central frequencies while these are normally distributed along x = y. This results in a convolution of this two broadening factor the homogeneous one which is isotropic in respect to these two directions and the inhomogeneous one that only affects direction x = y. If $\sigma \gg \gamma$ the result of this convolution changes from being a mixture of a Lorentzian profile and a Gaussian one to resembles to the original Gaussian distribution that causes the inhomogeneous uncertainty. Figure 3.2 graphically shows the reality of such interpretation. The sum of many many N Lorentzian bells with normally distributed centers tends to a much broader convoluted lineshape that resembles, for large σ, the Normal distribution from which the means of the Lorentzian bell were distributed. In the end, the two cuts in most case let the scientist retrieves the γ factor, related to the dephasing time, from the anti diagonal cut and from the main diagonal cut the σ factor to quantize the coupling with a bath interactions.

Letting t_2 to grow and studying at each 2D spectrum map the lineshape experimentally evolves to resemble a circle with the diagonal cut that shrinks and the anti diagonal broadens [20]. This effect is called Spectral Diffusion and it can explained considering that during t_2 the value of the molecule-bath interaction becomes less and less correlated to the one present at the absorption process. Those two values are eventually completely uncorrelated and the uncertainty looses its anisotropic character. Namely the broadening along x=y is as probable as along any other direction. The system uncertainty is then well approximated to a different pure Lorentzian. The simulation of the presented model does not show any of these evolution, there is no in fact any t_2 dependence. To quantitatively describe the Spectral Diffusion, the uncoupled broadening model by itself is not enough. Theory and algorithms have been then developed to find quantitative parameters to describe the spectral diffusion dynamics without changing the functional of the response functions. The Central Line Slope algorithm is an example of it, it has been specifically developed for 2D spectroscopy measurements and it is able to extract a time constant of the process even applied on quite complicated maps[22], [23]. A more general approach let to simulate those systems looking for more general response functions formulation not

only to extract an empirical quantity. The new equations come firstly with uplifting the hypothesis of uncoupled timescales for the two broadening processes and secondly developing a theory for a comprehensive lineshape function that might predict an evolution for t_2. The new model does limit to describing spectral diffusion but in certain condition and only for the excited state signals it also comprehend Stokes shift effect. In the end, the two distributions introduced above are retrieved as limiting cases of the generalized lineshape model.

The equations of next section will directly include also the response functions describing photo-induced absorption process. Albeit being described in the Theory's chapter, such interactions need a three level system model to happens. The model thus ought to include a second excited level to bring the total number of states to three. The second excited level can be introduced in the system Hamiltonian in many ways, here the most simple one is taken. A new parameter describing the energy gap between the first and the second excited states is introduced. But as unphysical as it can be, all the other parameters, formerly describing only the first excited state, are just exploit also to describe the newly introduced state. Photo-induced absorption signals can be then introduced bringing a negative contribution to the overall response function. For long in the following discussion, the third level really only stands as a proof of a certain scalability of the simulation towards more complex physical systems. In the last section, the second excited state comes strongly in to play to introduce vibronic coupling between excited states.

3.2. Implementing the brown oscillator model and analysis of results

This section aims to investigate the effectiveness and the physical meanings of the simulation based on the continuous Brown oscillator model. The analysis will focus on the parameters dependence and the model's capability to simulate newly introduced t_2 dynamics processes. At first a qualitative description of the simulated maps will be presented, then more quantitative measured are tempted to describe the Stokes shift effect, the spectral diffusion and the overall peak evolution from the perspective of t_2 time axis.

Response functions are computed upon the equations from 1.26 to 1.35. The lineshape function is, as presented and discussed in the first chapter, given by the Equation 1.33. From the simulation point of view, the only restriction to be taken care is the high temperature limit adopted during the formal derivation. A focus it will be instead given to the model's parameters, their physical meaning. Their role in the simulation results

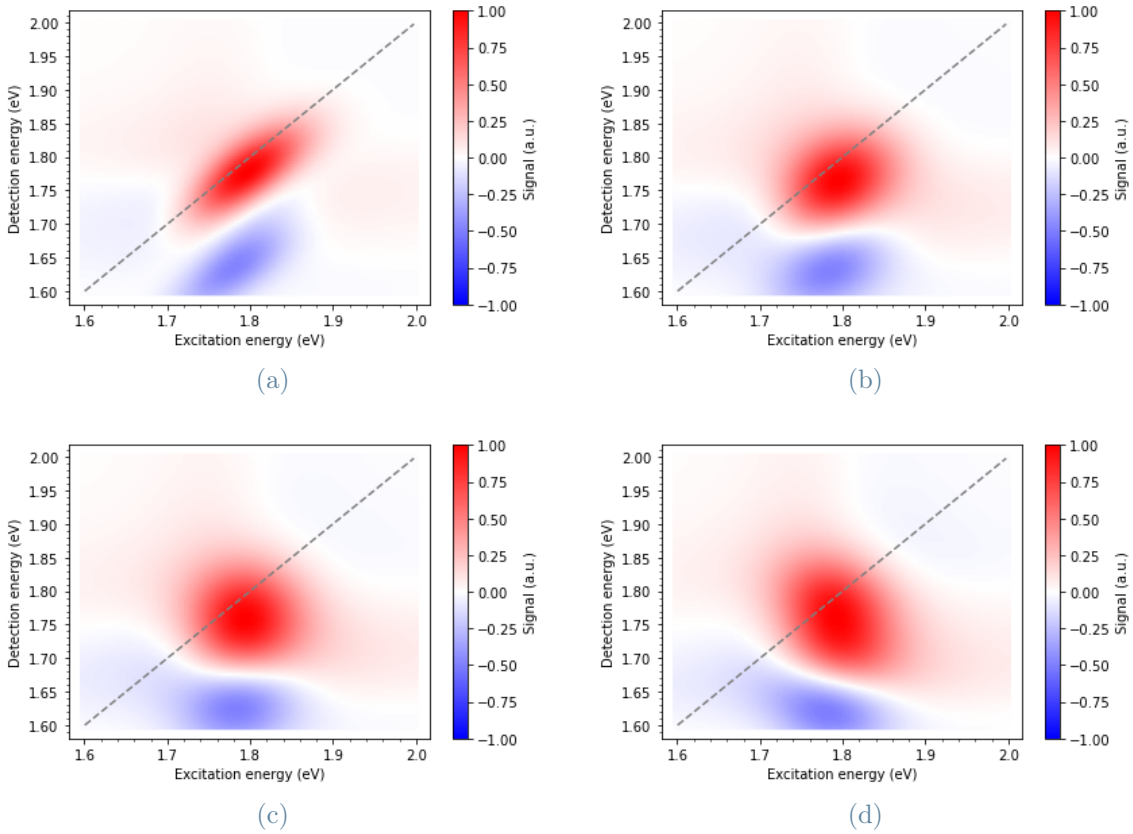

Figure 3.3: Examples of simulated maps of the Brownian oscillator model for three level system (3LS). (a)$t_2 = 0fs$(b)$t_2 = 50fs$(c)$t_2 = 100fs$(d)$t_2 = 500fs$ For all maps the model parameter were set as: $E_{01} = 1.8eV E_{12} = 1.65\lambda = 0.05eV\tau_C = 500fsT = 300K$

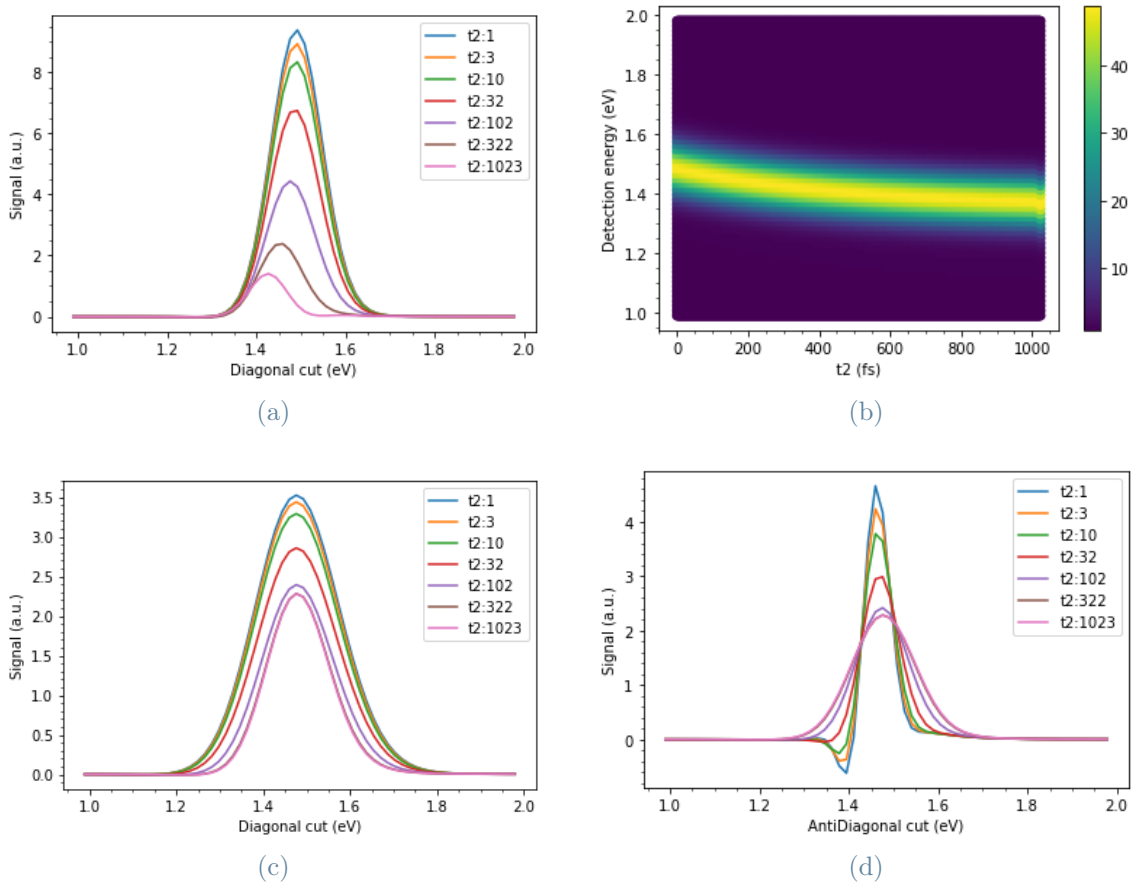

(a) (b)

(c) (d)

Figure 3.4: The model incorporates Stokes shift and Spectral diffusion: (a)(b)for the stimulated emission the Stokes shift is regulated by λ, in this case $\lambda = 0.1eV$; (c)(d)for the photobleaching the Spectral diffusion comes from a combination of the parameters, in this case: $\lambda = 0.3eV, \tau_C = 100fsT = 300K$

will be in fact emphasized within the discussion. Looking at the lineshape function $g(t)$, equation 1.33, three parameters can be recognized. Here they are listed in the formulation and unit of measure used in the simulation, trivial manipulation and unit conversion are then to be adopted:

- T, for Temperature [K]
- λ, giving the amplitude of the fluctuations [eV]
- τC, giving the coherence time related to the nuclear dynamics [fs]

Figure 3.3 shows in once an example of the lineshape evolution and the coexistence of the three modeled signals. The maps are now much more complex to characterize in respect to Figure 3.1, nevertheless they look more close to represent an experimentally measured spectrum where for example the lineshape keeps evolving during t_2 . As anticipated, the description will start from more qualitative aspect, approaching more technical and quantitative analysis later in this chapter. Figure 3.3 contains maps from the same simulation stopped at different t_2 time instants. Starting at $t2 = 0fs$, figure 3.3a, two different peaks can be noticed, the one on the main diagonal of positive amplitude and the other having negative amplitude. The two peaks represents three signals contribution, here as in other sections of this work, the three signal are referred for brevity as PB, photo bleaching and SE respectively for the stimulated emission, for the ground state photo bleaching and for the excited state photo induced absorption. Photo bleaching and stimulated emission gives positive signals and there are both centered around the 01 transition energy on both axis. The PA is detected at the 12 transition energy for a system excited at 01 transition energy, PA is in figure 3.3a responsible for the out of diagonal peak. The model then predicts a certain evolution of the the lineshape, that is in general expected and completely new compared to the previously presented model. The maps in figures from 3.3a to 3.3d evolve with the population time t_2 making possible to characterize experimental data with a single running model. As foreshadowed with theoretical arguments, the evolution along t_2 makes the lineshape more round and a dynamic shift can be seen looking at the diagonal peak projection on the detection energy axis. This shift it is called Stokes shift and it can be measured in almost every spectroscopy experiment of molecular sample [24]. With an experimental point of view, the presence of a noticeable Stokes shift makes possible to individually analyse stimulated emission and photo bleaching, that were previously completely overlapped. Figure 3.4 shows as such theoretical arguments find confirmation in the simulation. Figure 3.4a and Figure 3.4b contains different prospective of the same stimulated emission signal. The stokes shift can there easily spotted and eventually quantified in terms of the model parameters. Figure 3.4c and Figure 3.4d instead show how

well the spectral diffusion can be characterized from the two different cuts on the single photo bleaching contribution. As a matter of fact the lineshape rounding evolution, that the 2D maps showed, comes from an opposite tendency of change insisting on the two diagonal cuts.

In the following paragraphs, quantitative investigation exploiting these visualization techniques are performed. Simulations are run with each free parameter at a time changed against a fixed set of the others. Every parameter has been varied within a log-spaced interval. The boundaries of such interval are fixed to comply with the high temperature limits and the processes' time-scales overlap as presented in the theory. In addition, physical meaning has also been considered while fixing the boundaries.

3.2.1. Spectral diffusion modeling:

In this section spectral diffusion is described exploiting the parameter dependency analysis to deep the understanding of the phenomenon. From a phenomenological point of view the diagonal FWHM shrinks while its perpendicular counterpart grows. The investigation will be focused on the amplitude of the two FWHM and the time constant of their evolution. For simplicity the calculations are performed only on the photo bleaching signal. The main reason is that photo bleaching peaks close to the diagonal crossing with negligible shift for different t_2 nor other parameters. That makes easy to extract the FWHMs and it gives a stationary frame of reference to compare the intensities. For each parameters a set of figures has been chosen to guide discussion and as an evidence of the simulation results.

The reorganization energy, λ, is the first parameter to be singularly analyzed. The first two maps of Figure 3.5 give an insights of it, being the second line-shape noticeably wider along both direction. As Figure 3.5e shows at $t_2 = 0$, the main diagonal profile is much more broader than the anti-diagonal ones and the difference increases with λ. This reflects the predominance of inhomogeneous broadening for small t_2. At the opposite end, after long t_2, the two quantity are being equal and grow as much when increasing λ, Figure 3.5f. Looking at the Spectral Diffusion time evolution, the correlation between the time constant and λ seems close to zero. In the model in fact the time dependent part of the line-shape function does not depend on λ. For all those reason, it can be inferred that λ positively contributes only on the strength of the energy gap fluctuations: for bigger λ, the energy gap uncertainty increases both at the short and long time limit.

The same analysis applied for λ has been performed forτ_C, with quite different results. At first glance, from the $t_2 = 0fs$ map, Figures 3.5a and 3.5b, can be inferred that

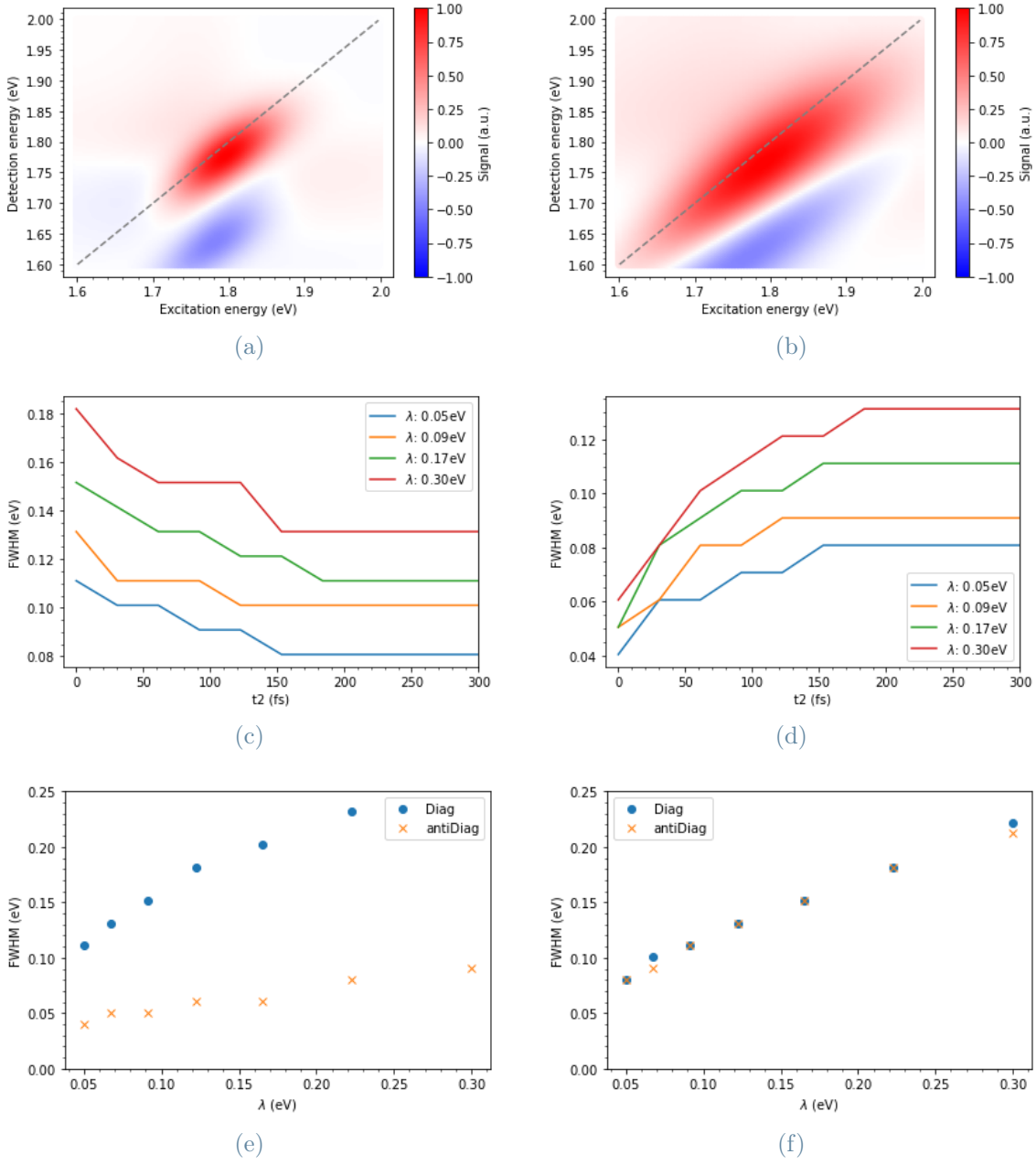

Figure 3.5: Changing λ has a striking effect on the lineshape. (a)(b)Simulated maps of photobleaching at $t_2 = 0fs$ for respectively $\lambda = 0.05eV$ and $\lambda = 0.20eV$. (c)(d)Diagonal and antidiagonal profiles evolve differently depending on λ, while the first shrinks the latter broadens to a unique regime value. (e) In the short time limit, $t_2 = 0$, the simple Gaussian inhomogeneous description is retrieved, while in the long time limit (f), $t_2 = 500fs$, diagonal and antidiagonal profile are as broad retrieving the pure Lorentzian broadening.

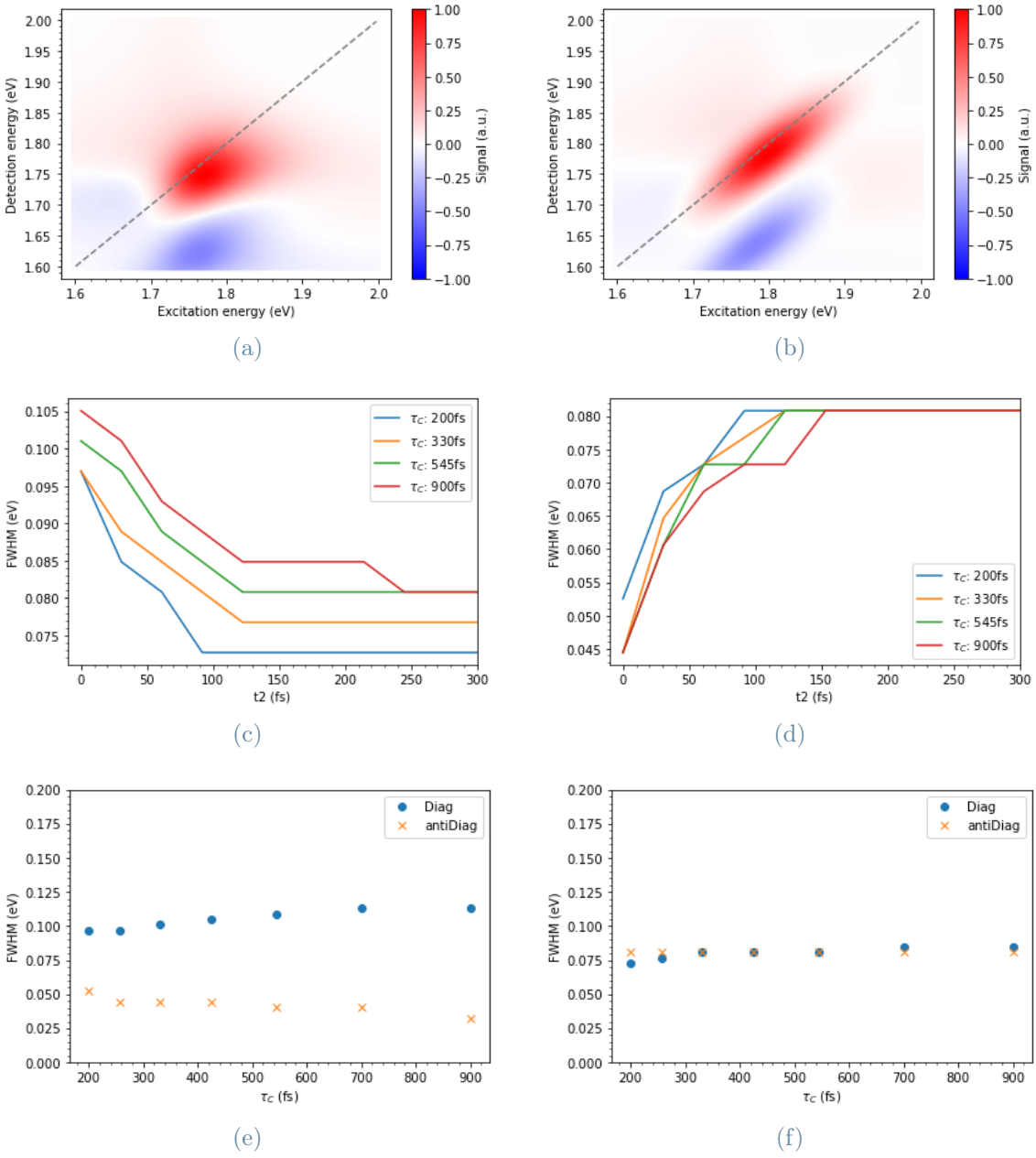

Figure 3.6: τ_C has a subtle influence on the lineshape. (a)(b)Simulated maps of photobleaching at $t_2 = 0fs$ for respectively $\tau_C = 100fs$ and $\tau_C = 1000fs$. (c)(d)Diagonal and antidiagonal profiles evolves with a different time constant, set by τ_C. (e) In the short time limit, $t_2 = 0$, for bigger τ_C it grows the inhomogeneous character of the lineshape, while in the long time limit (f), $t_2 = 500fs$, τ_C has no influence on the lineshape, this happens when the bath interaction is no more auto-correlated

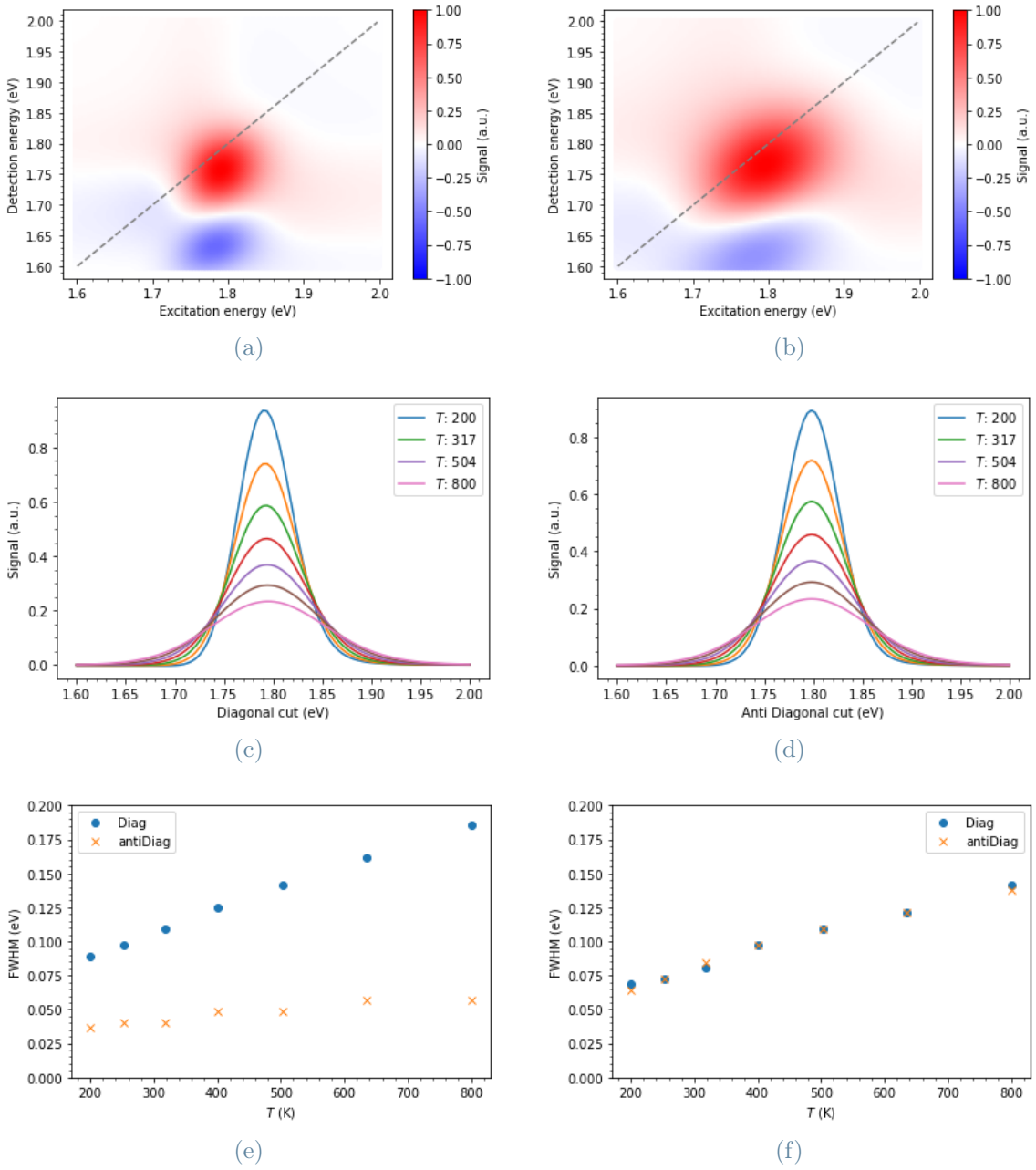

Figure 3.7: As it concerns to the spectral diffusion, temperature, T, has the same effect of λ. (a)(b)Simulated maps of photobleaching at $t_2 = 0fs$ for respectively $T = 150K$ and $T = 400K$. (c)(d)Diagonal and antidiagonal profiles depends on T as they do on λ, only their regime value is affects while the time constant is not (e) In the short time limit, $t_2 = 0$, for bigger T the lineshape broadens inhomogeneously, while in the long time limit (f), $t_2 = 500fs$, the homogeneous case it is retrieved with T affecting the electron dephasing time.

τ_C positively contributes to the narrowing of the peaks towards a pure in-homogeneous case. This is quantified by the second row graphs: the effect thus is negligible since the difference calculated on y-axis is very close to the energy resolution of the simulation. With that in mind,τ_C seems to affect the two profiles differently. The diagonal is generally increased whenτ_C grows while its counterpart slightly decreases if it does not just stay constant. The last row helps retrieving the role ofτ_C in the simulation. τ_C alone controls the time dependent part of $g(t)$, 1.25 and the graphs confirms that the time constant of the spectral diffusion process is positively influenced by a growing τ_C. Therefore τ_C gives an information on the time instant when the correlation of the energy gap values is loss. In others words, τ_C tells the scientist when the bath interaction at excitation retains no influence on the interaction energy at the detection. When no influence is retained the line-shape is circular.

As for the Temperature dependence the result of the analysis are compliant with the ones for λ. The correlation is as well positive even though not as strong. Such behavior it is completely justified by theory but by any means it implies that keeping independent Temperature and λ is redundant within the model. Temperature has very clear and defined physical sense, but from the simulation point of view its individual role shows up when analyzing the stoke shift effect.

3.2.2. Stokes shift modeling:

Stokes shift effect is a common feature of molecules in solvent. The difference in energy of the absorption peak versus the fluorescence one gives the values of the Stokes shift, and studies have been brought up to relate such value to the solvent reorganization energy affected by, among others, the solvent polarity and its influence on the energy landscape of the molecule. In this paragraph λ will be interpreted as the reorganization energy and its role together with the other parameter will be investigated. Analysis will be performed isolating the stimulated emission signal and measuring the evolution of difference along the detection energy axis of the peak at $t_2 = 0$ and at long t_2 limit.

The Stokes shift intensity heavily depends on λ at each time instant. As expected, Figure 3.8 shows the detection energy relative to the Stimulated emission peak shifting with time toward lower values. After a time interval, seemingly independent from λ 3.8a, a regime value, namely the Stokes shift energy. To check the linearity of the relation between the Stokes shift value and the reorganization energy that caused it, the two variables have been plotted in Figure 3.8d. Theory predicts the Stokes Shift being the double of the reorganization energy: the simulation works along such prediction with a negative offset

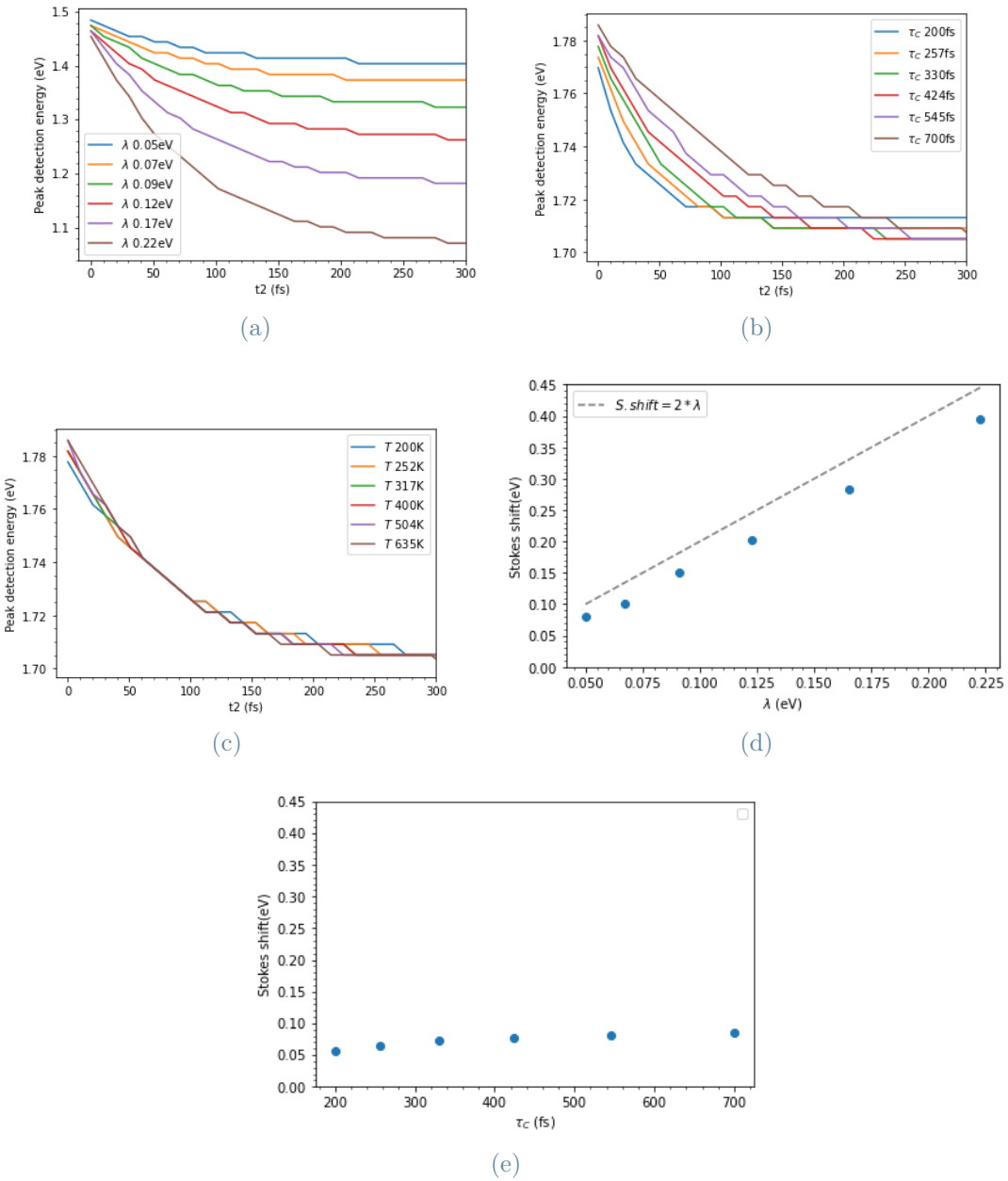

Figure 3.8: The three parameters τ_C, λ, T have a different impact on the Stokes shift. The stimulated emission peak's detection energy evolution is taken as quantitative measure.λ regulates the shift's amplitude (a) ,τ_C the evolution time constant (b) and T does not influence the Stokes shift which is an inherent chemical property of the sample.

of roughly 0.02 eV. Such fit has been tried also for τ_C with opposite results. Indeed λ alone completely controls the of the stokes shift value of the model.

Changingτ_C, one can discover different effects in respect to λ. While the Stokes shift values all end up very close to each other, the system reaches the regime value only after an exponential dynamics that clearly depends on τ_C. Again this is only a confirmation of the predictions inferred from model's equation, but also it points out that, in the long time limit, the complex part of lineshape $g(t)$, responsible of the Stokes shift, depends only on λ.

The temperature turns to have no visible effect for the Stokes shift, neither on its value nor on the dynamics that regulates it. This comes straight forward from model's equation and it confirms that the Stokes shift value only depends on the solvent-solute properties interaction and not on the energy available from the thermal bath.

3.2.3. Signal peak's amplitude decay:

The last analysis performed for Brownian Oscillator model is the decay of the signal. To do so at first the max value of the map at each time instant is taken as the control variable to follow the evolution of the peak even when its energy coordinate changes. This makes possible to compare the photo-bleaching decay to the stimulated emission one: the result is a complete match of the decay dynamics. Same works with opposite sign for the photo induced absorption. Following the structure used so far, the parameters influence is singularly explained with the aid of Figure 3.9.

Despite being less significant in terms of experimental evidence, studying the decay of the signal due to bath interaction uncorrelation proves to be necessary for a deeper understand of the model. For the sake of the signal decay discussion, what is inferred to λ is to be inferred to the temperature as well. As Fig. 3.9a and Fig. 3.9b show, the reorganization energy λ does not affect the dynamics of the decay, but only the initial and final value. This can be visualized better when the signals for different λ are plot without first normalizing to their maximum value, as in Fig. 3.9a. Once more the initial and the final signal intensity are negatively correlated to λ, this is easily explained by the normalization of the response function. To a broader response always correspond a smaller maximum amplitude so that as a probability distribution density its volume stays normalized.

Furthermore, re-normalizing every signal to its maximum really makes easy to verify that the time constant of the decay process is positively correlated with τ_C as in Fig. 3.9d. Time constant it is fact given by $\tau_C/(2 * \pi)$. Regarding the different signal drop for different values of τ_C, the same arguments of the broadening of the overall signal are to

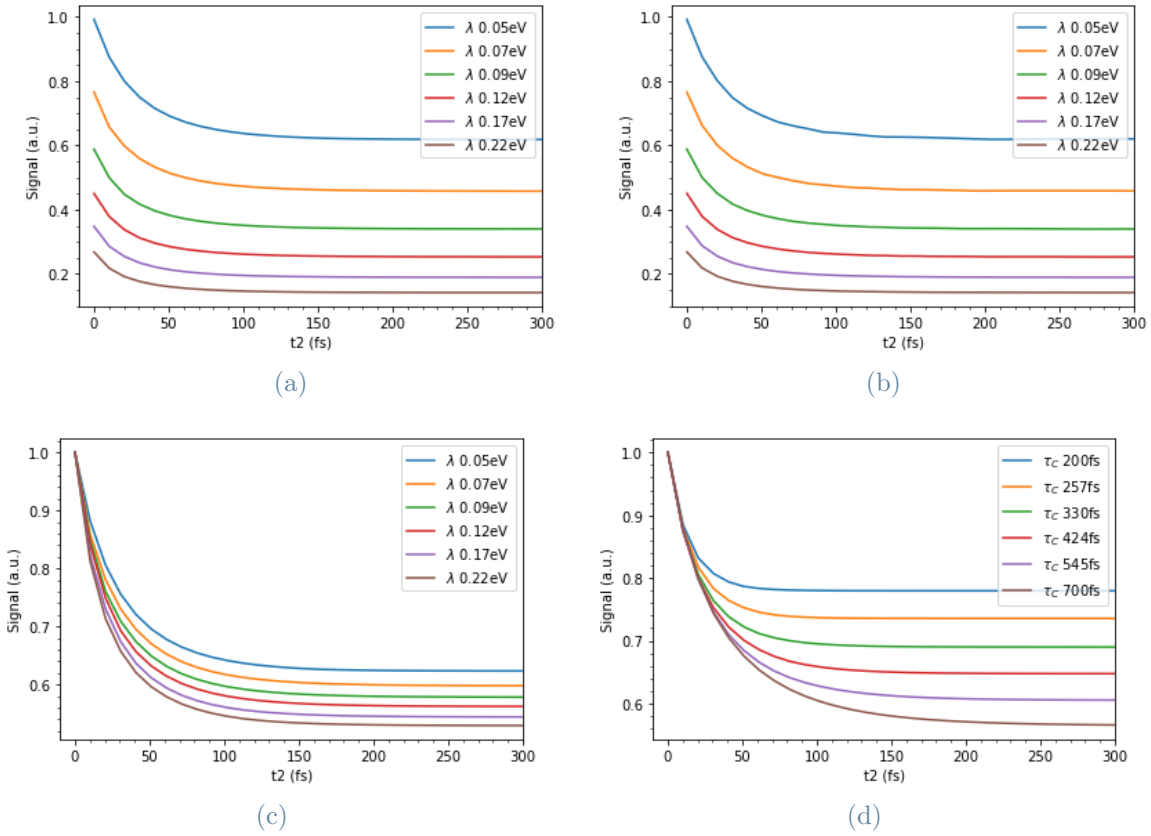

Figure 3.9: All of those figures show the dynamics of the maximum signal intensity, regardless its position in the map. The photo bleaching signal in (a) decays equally to the simulated emission signal in (b), regardless a change in λ. Re-normalizing the photobleaching dynamics allows new perspective. The signal drop, in proportion, grows with λ, (c), while once again τ_C defines the time constant.

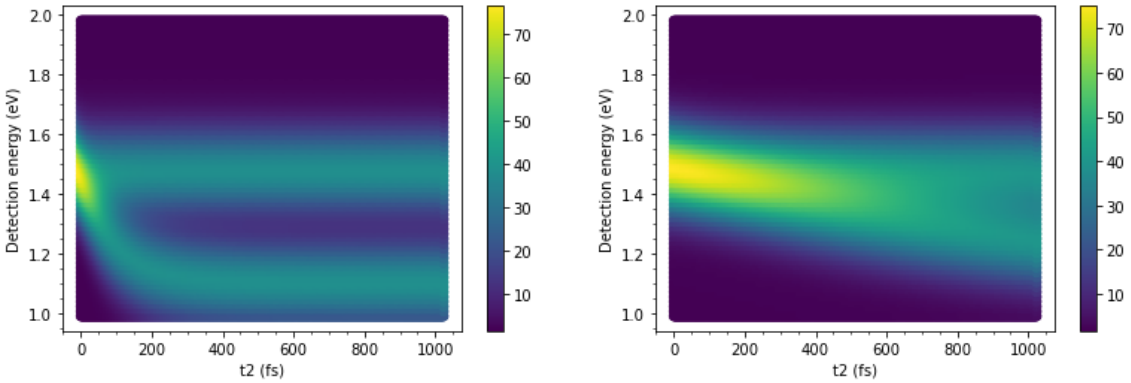

(a) (b)

Figure 3.10: The 'pump probe like' map offers a mean to visualize signal decay and Stokes shift. For (a) $\lambda = 0.1eV, \tau_C = 100fs$, (b)$\lambda = 0.1eV, \tau_C = 1000fs$. The time constant evolution of both processes depends only on $\tau_C = 1000fs$, in fact τ_C does not tell anything about the specific process, but it acts as re-scaling factor for the t_2 time axis for the full response.

be apply. As it was found in the spectral diffusion paragraphs, τ_C, although smaller, has an impact on the broadening. Beside the diffusion process no other decay effect along t_2 have been modeled, so every signal after the decorrelation process lives beyond the studied timescale, this can be verified for all the subplots of Fig.3.9. Another aspect the model fails to introduce, it is differentiating on how the bath interaction affects the ground state or an excited state. The stimulated emission peak in Fig.3.9b evolves exactly like the photobleaching one. This is no false in general, but in most cases experiments tell differently.

Those paragraphs have explained how the three presented parameters plays a role in the simulation results. The data obtained succeeded reflecting the math behind the model, the analysis pointed out the various phenomena the model is capable to predict and they explained the physical meaning of the various degree of freedom the model presents. As an example, parameterτ_C is found to regulate the time dynamics of different aspect of the simulation data. As counter intuitive as it could be, all the phenomena presented follow from the sample with its dephasing time being coupled to a stochastic evolving bath. Such reality is shown all together in Fig.3.10. These pump-probe like maps let visualize signal decay and the stokes shift within one plot, clarifying how coherence timeτ_C seems to regulate the time constant of both effects. Keeping the same λ and T, both the stokes shift dynamics and the signal overall decay are made slower, just as time axis has been re-scaled. For the sake of completeness, not all parameters have been investigated. For

each response function there is multiplying scalar that has been for the mean of the simulation set to 1. Changing the re-phasing and non re-phasing amplitudes can modify the line-shape to better fit some experimental data, in general changing those scalars has not influence on the functional behavior of the signal.

3.3. Implementing vibrational degree of freedom, vibronic coupling and relaxation

3.3.1. Pure vibrational model implementation and analysis

Nuclear vibrations and electronic coherent oscillation are well known physical realities and theories of many kind have no problem to predict and explain them. A precise description of the dynamical interplay between electronic and vibrational degrees of freedom plays an crucial role for understanding many photo-physical processes[9]. Multidimensional spectroscopy represents a powerful investigation tool to characterize dynamical light-matter interaction and different theoretical models can guide for a better understand of such complex interconnection. Vibronic couplings, an-harmonic terms in the Hamiltonian and different curvatures of the energy levels are only few examples of how the different degrees of freedom can be reciprocally affected. In this context, following the work of F.E. Quintela Rodriguez and F. Troiani[9], the displaced oscillator model will be analyzed. Often times the dominant contribution of electron-vibrational coupling can be explained in terms of such model. From a simulation point of view this model keeps the electronic Hamiltonian and the vibrational one separated in terms of variable so the resulting response functions would be a product of the two. For a more meaningful discussion in this work the non-vibrational response function will be the one modeled in the last section. This choice could raises issues with the coherency of the two model. In developing both models, assumptions have been made and result might not be of a meaning at all. A striking example is the temperature limit. The theory developed for the stochastic brown oscillators model is supported by the high temperature limit, while the theory underneath the displaced oscillator model is developed at T= 0 K. To reconcile the two models a generalization of the displaced oscillator model has to be done. Such generalization though leads only to add a scalar term, temperature dependent, in front of each response function simply re normalizing the whole signal. More complex, and yet to fully understand, is the description of the electronic states in terms of nuclear coordinates, on one side the displacement is parameterized with the reorganization energy λ and the harmonic oscillators form a continuous of infinite modes. On the second side the oscillators are displaced

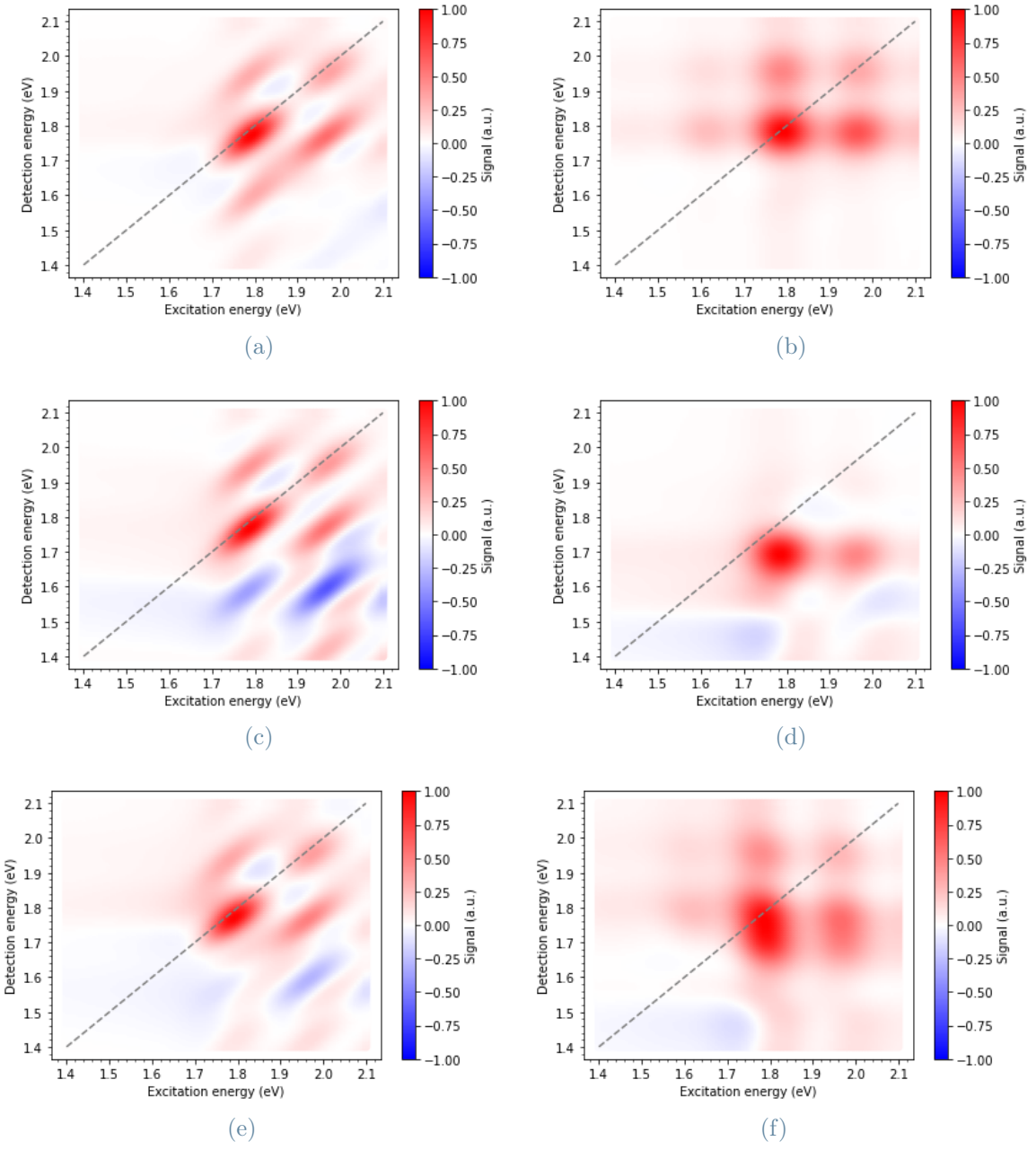

Figure 3.11: Simulated maps for the vibrational model, parameters: $E01 = 1.8eV \lambda = 0.05eV \tau_C = 500fs T = 300Kz = 0.7\omega_\nu = 0.17eV \tau_V = 1000fs$. $t_2 = 0$ for (a)(c)(e) $t_2 = 500fs$ for (b)(d)(f). Maps (a)(b) contains only the ground state contribution, (c)(d) the excited state contribution, (e)(f) the sum of it as it would be measured experimentally. The partition give a means of understanding the cross peaks nature based on their position

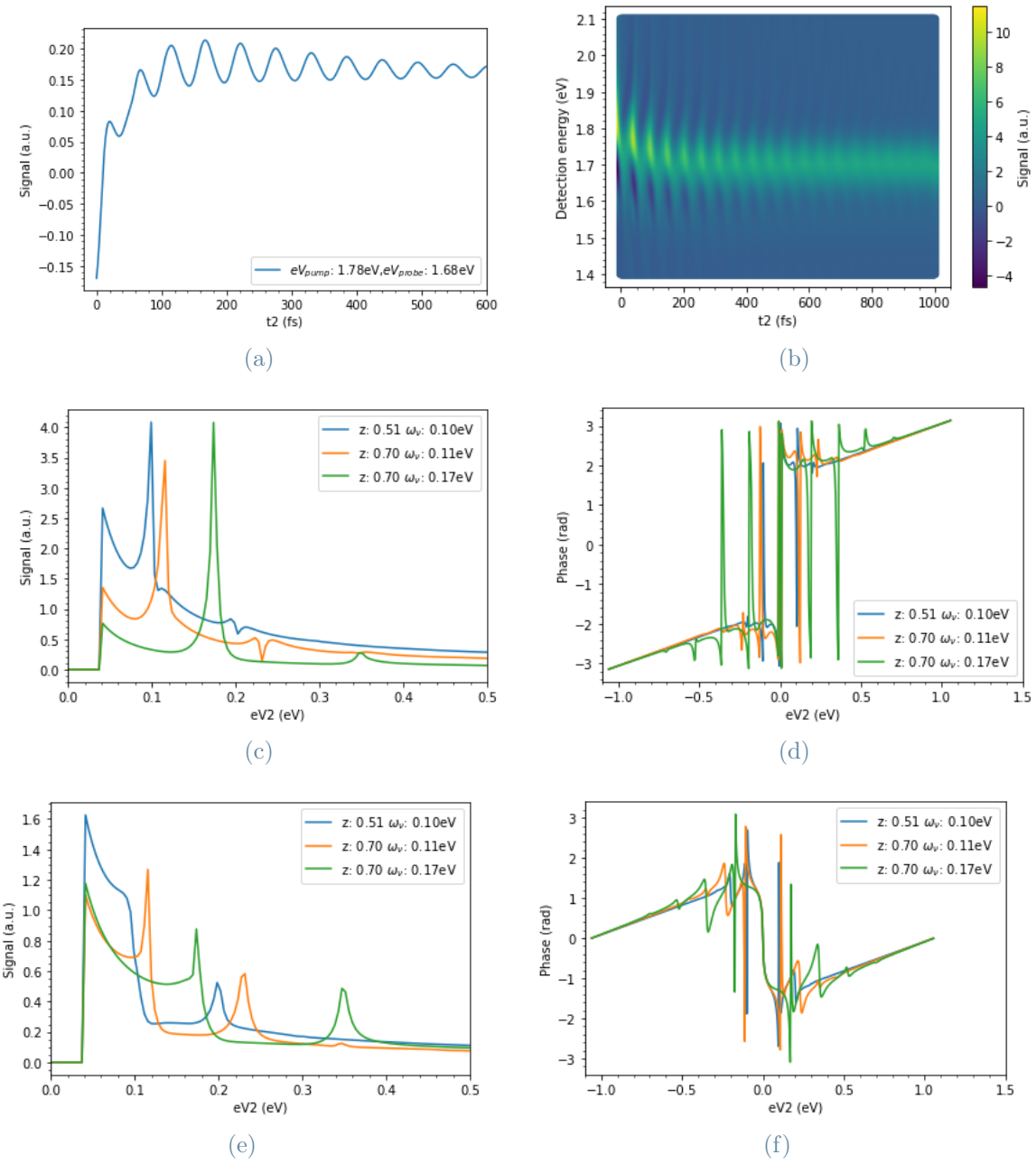

Figure 3.12: Vibronic interplay coincides with an oscillating response function along t_2. (a) shows the Stimulated emission peak dynamics for $z = 0.7\omega_\nu = 0.08eV\tau_V = 1000fs$. The oscillating modulation can be seen also for the pump probe like map in (b), a non trivial phase relation is to noticed within the wave front.(c)(d) contain the Fourier transform in amplitude and phase of the stimulated emission signal. (e)(f) contain the Fourier transform in amplitude and phase of the photobleaching signal. While the mode energy depends on ω_ν, for the photobleaching the contribution of the overtones increases with 'z' while for the stimulated emission it stays negligible

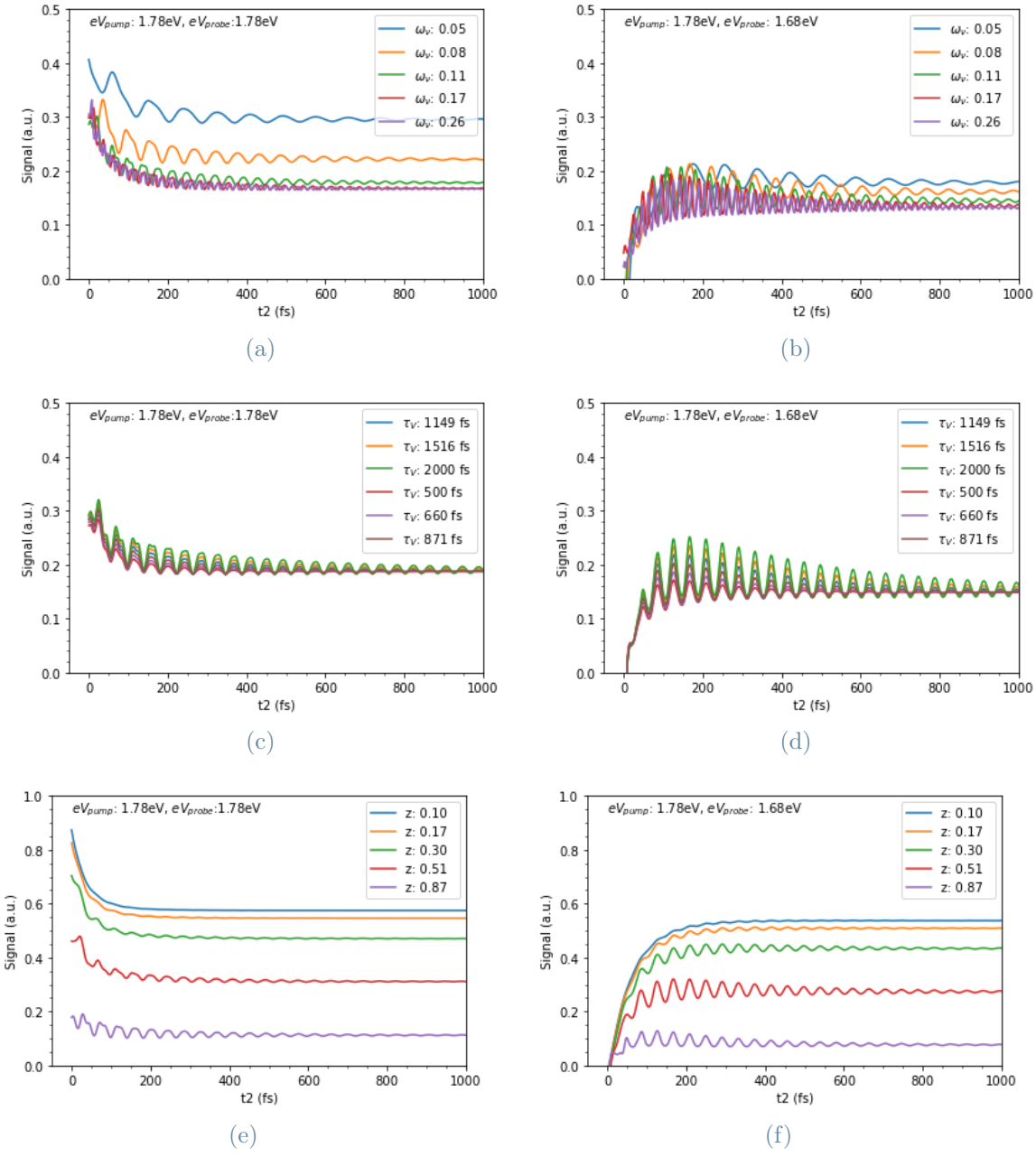

Figure 3.13: As for the Brownian oscillator model, three parameters: the displacement z, the quantum of vibrational energy ω_ν and the vibrational relaxation time constant τ_V =. Their impact has been investigated for the photobleaching in (a)(c)(e) and for the stimulated emission in (b)(d)(f). 'z' shows a non intuitive dependence and its role will be further analyzed.

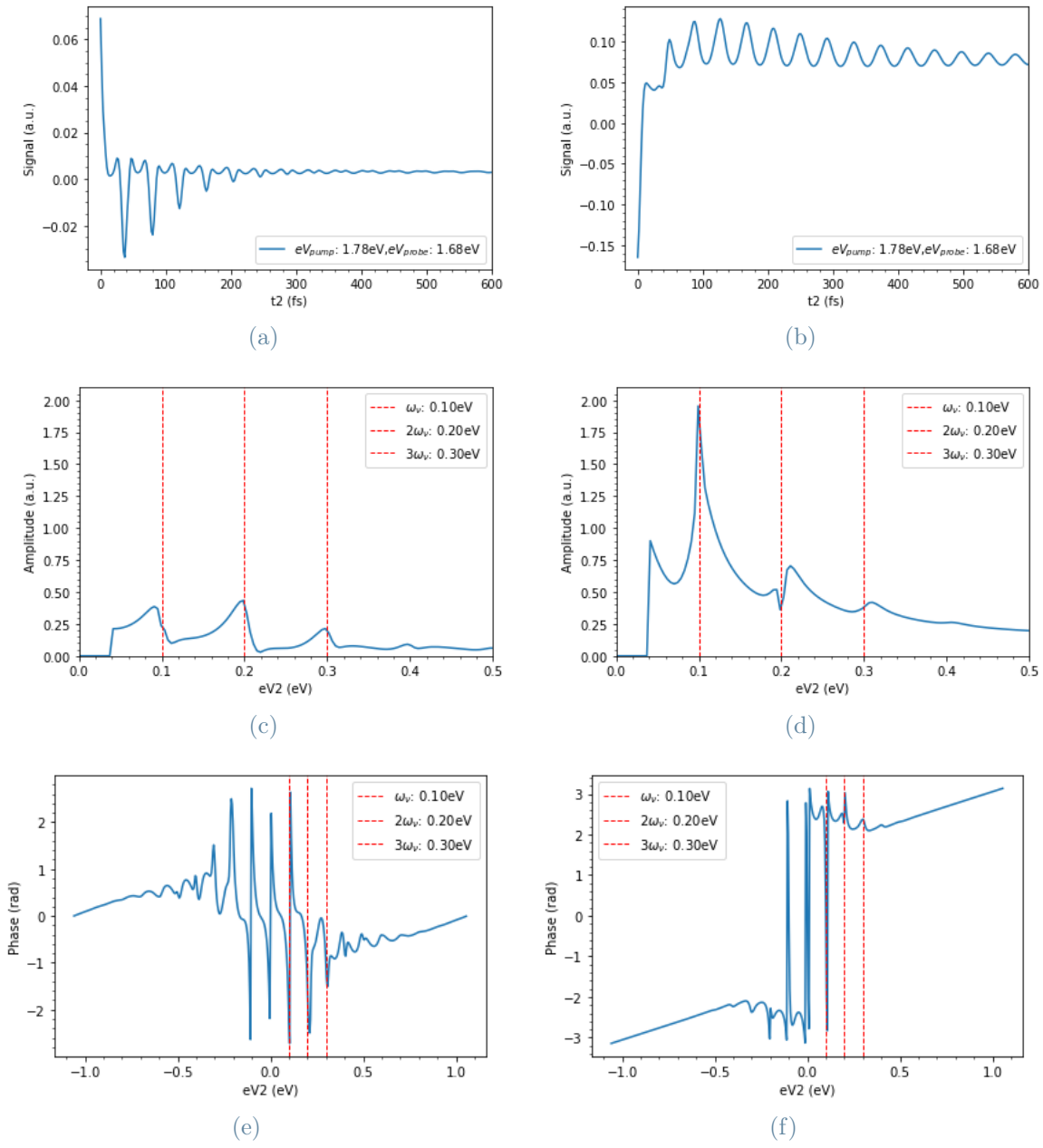

Figure 3.14: for a fixed couple of $\omega_\nu = 0.1eV\tau_V = 1000fs$, $z = 1.5$ for (a)(c)(e) and $z = 0.87$ for (b)(d)(f). As it seems from the simulation they both are high value for 'z' but only on the first case the effect of the dynamics it is quite dramatic. The first overtones contributes almost as much (c) and phase becomes very noisy (e). These combined explain the unexpected dynamics in (a).

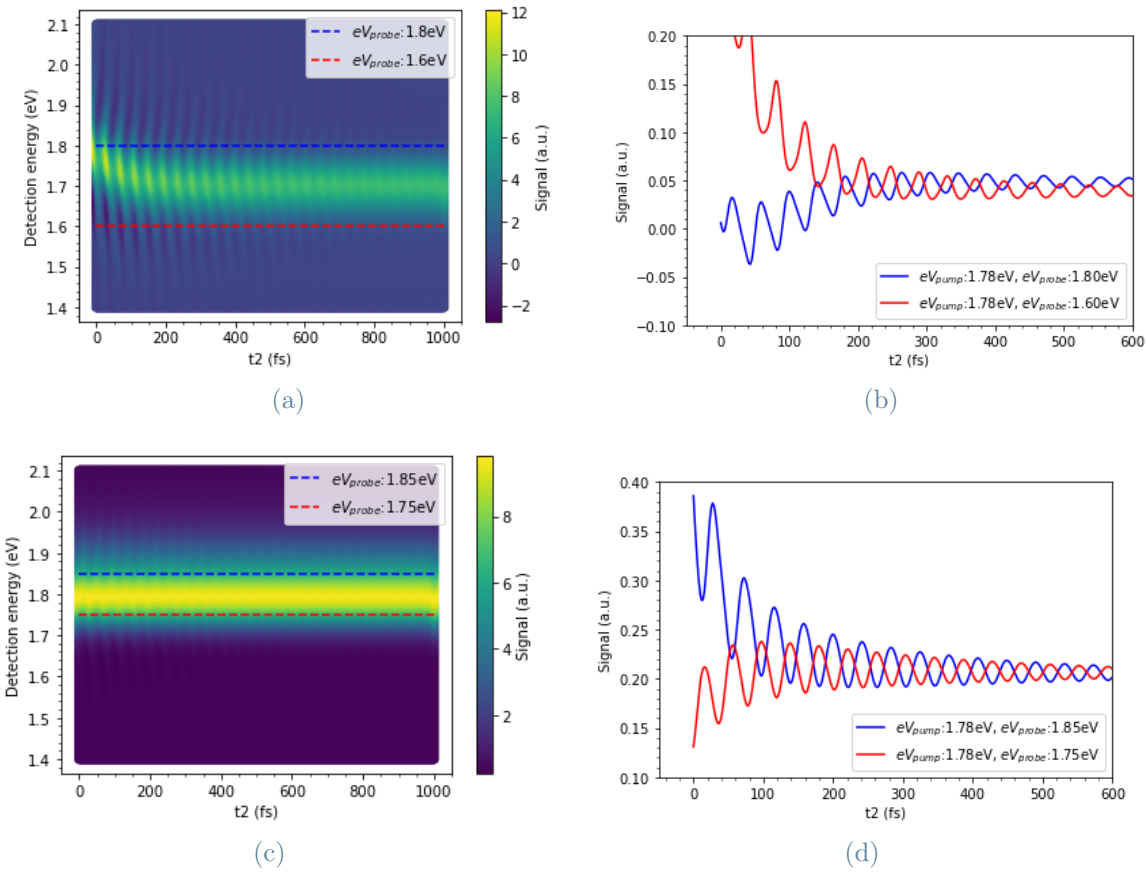

Figure 3.15: As it can be notices from the pump probe like maps, (a) for the simulated emission and (c) for the photobleaching, the wave front it is plane. That is to say that the dynamics of points taken across the main peak show a non trivial phase relation, in fact they are in general counter phased. Such relation will be investigated also on the experimental data set

by the factor z and vibrations come from a discrete single mode. All of this is justified from a phenomenological point of view, the features introduced by the two models can be considered independently. Secondly, Brown oscillators model the interaction of the sample molecule with the environment, from here the continuous mode hypothesis and the stochastic description, while the displaced oscillators provide a source of inter-molecule nuclear-electronic interaction and the vibrational mode considers the sample molecule nuclear coordinate. A qualitative analysis of the correlation of the vibrational dynamics with λ has been performed and it will be shown later in this section. As a final modification of the implemented model, the vibrational mode has been also characterized by a decay rate to model the pure nuclear relaxation that the system might undergo and to reproduce more realistic results.

The 2D maps of the simulation of both model very much resemble the maps of the previous chapter, all the main features are maintained: the peak's line-shape evolves as modeled with spectral diffusion and stokes shift that can still be quantitatively characterized. The cross peaks are though a consequence of newly introduced vibrational Hamiltonian. They are in fact a part from the main peak of roughly the vibrational quantum of energy (e.g. $\omega_\nu = 0.23$eV). The model considers an infinite amount of higher tones replica and those would have been seen if the energy spectrum spam were broader. Most of experimental setups measures the sum of all response functions along the detection direction, maps like the ones of Fig. 3.11e and Fig. 3.11f are then obtained. The simulation makes separating the stimulated emission signal from the photo-bleaching very simple. As it was in the last chapter, the analysis here proposed exploit this possibility to distinguish from excited states signals, namely the stimulated emission, and the ground state signals, namely the photo-bleaching. This distinction is based on the kind of state in which the system stays during the delay t_2. As an evidence Fig.3.11c and Fig.3.11d shows the Stimulated Emission signal, while Fig. 3.11a and Fig. 3.11b the photobleaching. The maps suggest only the peaks at detection energy equal 1.8eV are shared between the signals: the ones above such energy comes from a photobleaching; the ones below comes from a stimulated emission. The cross peaks can be exploited to investigate ground or excited state signals individually also in the experimental set up. Several and dimmer cross peaks are seen on the maps of Fig. 3.11, as transition involving vibrational overtones they are characterized by lower Frank-Condon factor so they vanish for longer t_2. Those and all the replicas undergo the same line-shape evolution of the main peak, this suggests that the Brown oscillator model contribution to the response functions works as a modulation of the entire map, including the signals that purely comes by the introduction of the displaced oscillator model. This result strengthens the choice of adding the two Hamiltonian contributions independently.

This all comes from the assumption that the stochastic interaction does not depend on the excitation level of the system, considering both the electronic and vibrational excited levels.

The 2D maps give only a hint of the vibrations taking place along t_2. Only the main peak will be analysed and excited state's signals will be individually studied from ground state's one. The division will be of crucial interest when investigating an unexpected result of the simulation. Integrating over the excitation energy axis a pump probe like map is computed Fig. 3.12b, upon the already the stokes shift dynamics an oscillating modulation can be spot. At first glance the modulation can be characterized by three parameters: the oscillating period, a time constant to quantify the fading process of the coherent vibration and a non trivial phase relation along the Detection energy axis. The first two aspects are easily related to two of the simulation's parameters. The oscillating period is proportional to the inverse of the quantum of energy of the only vibrational mode present in the model. While the fading of the modulation is controlled by the pure vibrational decay rate specifically introduced in the model. Such dependence would be further investigated by a specific dependence analysis. The non trivial phase relation along the perpendicular to the propagation direction requires less straight forward arguments. The vertical axis stands in fact as the detection energy axis but it firstly represents the system evolution along t_3 in the frequency representation. Therefore while the system properly vibrates only in respect of t_2 , since only during t_2 its state reaches a population state either ground of excited, it retains a phase factor dependence from the evolution along the other two time intervals, namely t_1 and t_3 . More on this aspect will be analyzed at the end of this section and an experimental evidence of it is also presented. Sticking to the t_2 dynamics representation, Fig. 3.12a, the stimulated emission signal at the coordinate of stokes shifted peak. The raising dynamics comes from the shifting, and thanks to this representation the vibrational modulation can be also by its amplitude. No trivial dependence has been found for it, looking at the equations of the response function 1.38-1.41 suggest that the displacement 'z' controls the oscillation amplitude but this has no simple feedback on the simulation results. The same negative correlation is suggested by considering the oscillation amplitude as a function of a transition dipole between two states coming from different electronic curves, this dipole would be than proportional to the overlap of the two wave-function projected on the reaction nuclear coordinate. From this argument, increasing z should reduce such overlap thus reducing the transition probability amplitude. To further characterizes the dynamics, an additional Fourier transform can be applied on the t_2 axis. To best visualize the Fourier transform amplitude, an High Pass filter is applied to the signals with a cutoff frequency of $0.04eV$. The non filtered spectrum

presents in fact the greatest peak at the zero frequency component, the peak accounts for the raise and decay dynamical contribution than it is thus neglected. The remaining peaks should account for the excited vibrational modes. Even being quite noisy, due to the numerical approximation, each peaks can be found at the expected energy, namely the harmonic tones of the fixed mode. As it often happens, this can seen even more clearly looking at the transform's phase. The modulus of the transform though gives an insight of the oscillation amplitude, the higher is the peak the higher is the intensity (amplitude) related to that mode. Fig.3.12e and Fig.3.12c show how changing the energy of the quantum of the mode changes the position of the spectrum peaks, but changing z does not really influence the amplitude corresponding to that mode. Comparing the two figures the difference between ground state bleaching and excited state emission is evident and it can be investigated. First thing to notice is the fact that, keeping the same overall signal intensity, the vibrational peaks of the photo bleaching are halved compared to the stimulated emission ones. This will be further proven by looking at the dynamics in the time representation. In respect to the phase diagrams, the same evidence can be found comparing the peaks' intensity at the vibrational tones. The functional shape though looks different, at high frequency, negative or positive, the stimulated emission signal shows a phase factor close to π while the photo bleaching signal phase is close to zero. Besides this, both approaches the center of the diagrams in a similar way.

As presented for the line-shape section, a parameter by parameter analysis is shown here. The objective of such analysis is dual. First goal is to fully asses the model capability of simulate different signals and features that might come out from experimental data. Secondly and more deep goal is to relate the different dynamical characteristics to a controllable parameter deducing from such relation some physical meaning and more knowledge. The most simple parameter to start is the energy of the quantum of excitation of the vibrational mode, we refer to that parameter as ω_ν. In Fig.3.13a for photobleaching and Fig.3.13b for stimulated emission, signals for different ω_ν are shown. Starting with the Stimulated emission, the amplitude of the non vibrating response Function does not noticeably change. What dramatically changes is the oscillation frequency, this follows Plank's relation and it is very much expected from the simulation. Looking at the Photobleaching, beside the frequency dependence, a change in the response amplitude in the long time limit can be measured. The physical meaning behind this phenomena is yet to be fully explained but it could be retrace to a different normalization factor of the response function. This same argument is more easily applied to the z dependence study. Changing z, great changes are measured both in the overall response function amplitude and in the amplitude of the oscillations. While the first can be explained by a decreasing overlap

factor of the wave-functions, the amplitude of the oscillations follows a more complex rule. As suggested by the transform's amplitude diagrams no clear relation with z can be retrieved. In the Stimulated emission graph the oscillation reaches a maximum in amplitude around z = 0.7 to become for higher z narrower and more noisy. The same can not be state for the photo bleaching signal. Oscillations seem to grow in amplitude for increasing z, together with the amplitude of the oscillation a not expected noise or interference figure seem to increase, while for the Stimulated emission signal such interference appears only for high z. This effect can be caused by a non trivial phase relation between the overtones, this thesis is supported by the complexity of the phase diagrams and by the fact the in respect to the plot referring to the stimulated emission signal, the photobleaching has a more clear interference figure and higher overtones peaks in the transform graphs. Being do a simple overtones interference implies that the frequency of the figures is an integer times of the main tone frequency and that the interference pattern evolves to a simpler oscillation of the single main tone, which it has an higher specific amplitude thus it fades becoming negligible after longer interval. The overtones interference explanation has not explained why it affects more the ground state signal than the excited state one. This aspect will be further investigated on stimulated emission response dynamics at higher z. The last single parameter comparison regards the role of the decay rate of the vibrational tones, as referred as τ_V. The dependence on both signal is quite straight forward, the vibration gets dimmer modulated by a negative exponential function with a time constant that depends on τ_V. An unexpected characteristic of such effect that in respect to the assumed constant non oscillating carrier function, such decay only affects the upper side of the oscillation or, in more physical terms, τ_V affects also the non oscillating carrier's dynamics that would be more intuitively only dependent on τ_C, the coherency time constant of the Brownian oscillator previously discussed. This effect turns out to be more evident considering the photo bleaching signal's dynamics. Figure 3.13d in fact shows the existence of a positive contribution from both the parameters, namely τ_V and τ_C, to an overall effective time constant of the non oscillating part. This can physical defended, considering that in a non vibrating simulated model τ_C expressed the time interval during which the energy gap value it is well auto correlated, such correlation fades with time due stochastic changes of the environment and thus of the interaction strength. In the current model the energy gap does oscillate regardless the environment interaction, thus it introduces a non trivial correlation the process. When both effects are considered, the whole stochastic process shows a smaller correlation arguing for the possibility to define an effective coherence time instead of the previously usedτ_C.

In the next two paragraphs, two less intuitive and therefore worth of explanation results

will be discussed. The first topic the discussion will focus on is the interference pattern that it visible at the beginning of the ground state photo bleaching signal and it shows its self in the excited state one when z is increased. The analysis focuses on this latter aspect and it investigates the relation insisting with the displacement of the oscillators. Two cases, one with high z and one with higher z, of stimulated emission signals are taken as an example. There will be presented different explanation hypothesis, but no strong result can in be in fact shown or inferred. A first, intuitive, explanation would be to relate it to an error due to the numerical, thus discrete, nature of the simulation. The simulation used in fact a sampled representation of the response function but the sampling time interval is lower by at least an order of magnitude than the time scale of the interference pattern. Additionally as shown before the interference pattern has the same frequency of the vibrational mode, controlled by the parameter ω_ν, and ω_ν has nothing to do with the sampling time interval chosen. The time scale grows and shrinks following the oscillation period and not the sampling time, which it is kept constant for every simulation. The existence of an unavoidable error as a direct consequences of a numerical treatment is of course not under discussion. At the same time there are methods to asses the order of magnitude of such error and a good practice is to ensure that the order of magnitude of the simulated data at each step of the process never approaches such limit. Graphing the dynamics along t_2 of a response function it, computing cost wise, a very simple operation. The response function is directly defined along that variable axis and it does not undergo any transformation. For such operation the numerical error is given by the machine precision and to the representational power of the floating representation of number in use. As a first hand proof, the two dynamics stay well within the [-0.2, 0.2] interval and the variations investigated are at their minimum of the order of 0.001. With this undoubtedly rough and scholastic argumentation, explaining with representational error what it can be considered a noisy oscillation is excluded. The same trust should not be employed while extracting information from the graphs of the Fourier transform. This is due to the high number and the complexity of the manipulation needed to compute such results. This is the reason why the phase relation among the tones is messy and complicated could be in principle only accounted to the 'fast Fourier transform' algorithm used to extract it. Having, for the moment, excluded a numerical reason does not bring any closer to find an explanation, some open questions remain: what does it have to do with z? Why does it affect more the photo bleaching signal? What should one look for during a physical experiment to have an evidence of such overtones interference? Not satisfying explanation has been found throughout this work, a reasoning based on the physics of the model is here attempt. As the figure suggests the interference is caused by non coherent contributions of overtones. The complexity of the phase relation between overtones, as Fig. 3.14e and Fig.

3.14f show, increases with z. This is not related to a bigger number of overtones involved but it might be caused to a more spread amplitude within the excited overtones. In the Fig.3.14c and Fig.3.14d one can verify that increasing z reduces the overall amplitude of the signal but not the number of overtone non negligibly contributing. At the same time the amplitude ratio of the main tone and the first overtone seems to increase for a bigger z, in the extreme case of $z = 1.50$ the first overtone contributes more than the main tone. Coherently exciting overtones does not lead to such wave shape but the stochasticity, introduced to model the lineshape evolution, can be accounted for the finite phase relation between the main and first harmonic tones. A non zero phase difference leads in fact to such oscillating dynamics. Regarding the difference found for the photo bleaching case, the evidence of long lasting excited overtones it is supported by a comparison between the 2D maps in Fig.3.11b and Fig.3.11d. In fact at $t_2 = 0fs$ the two maps are comparable in terms of excited overtones. In the long time limit instead, the overtones seem to contribute to the overall signal dynamics more for the photo bleaching signal than for the stimulated emission signal. A 2D map gives not information on the dynamics along t_2 axis, but along t_1 and t_3 instead. Such information can be still considered of value when evaluating properties strictly related to a population state of the molecule. Being at an overall lower energy is generally a condition for a state to be more populated and even if the vibrational model does not include any consideration on thermal energy distribution in the system, the Brownian oscillator model does.

One last aspect is discussed, namely the counter phase relation between two oscillating dynamics of points taken across the main peak along the detection energy. A non zero phase relation along the detection energy axis has been foreshadowed looking, at the beginning of this section, at a pump probe like map. This aspect will be reprised while considering experimental data that clearly show the same feature. A simple way to detect on pump probe like map a non trivial phase relation along eV3 is to analyse the wavefront along that direction of the wave propagating along t_2 . If the phase were not depending on the detection energy the wavefront would look like as a vertical straight line as in the case of pure plain waves. This might seem at first glance to be the case of the photo bleaching signal, it will be shown later on that in fact the same counter phase and thus not trivial, relation insists equally to the stimulated emission signal and to the photo bleaching one. Looking it terms of Bode phase diagram of the response function of a simple dynamical system, this result is no surprise. Considering a system with one simple pole or two complex ones, moving across its resonant frequency the impulse response function gains a phase factor equal to π. This comes simply from mathematical arguments with no need of any special physical phenomena involved. With this is mind, the response function of

the modeled system has in fact two conjugated complex pole at the energy gap frequency, more over the dynamical model is simple enough so that the overall phase relation is just that one, and simply sampling the response function across the poles gives two oscillating dynamics with a clear phase difference of exactly π. In the figures two values on the detection energy axis are chosen to close to symmetrical from the resonant energy, so that the amplitudes are similar, and far enough that the phase transition is completed. This interval is in general related to the dumping of the oscillating mode as the stronger the dumping strength the slower is the phase the change. In the simulation the dumping parameter is regulated by τ_V and the phase transition is fast enough so that the counter phase oscillation can be recognized also at energy close to resonant. For example if τ_V was smaller enough, meaning the vibrations are very short living, the energy interval from which boundaries the points are taken might be too wide and no oscillation of any phase can be recognized. The complexity of the natural systems and the short living vibrational mode are very much present reason for why this effect is not so common to be measured on a multi dimensional experiment setup.

3.3.2. Phenomenological model for a non adiabatic coupling:

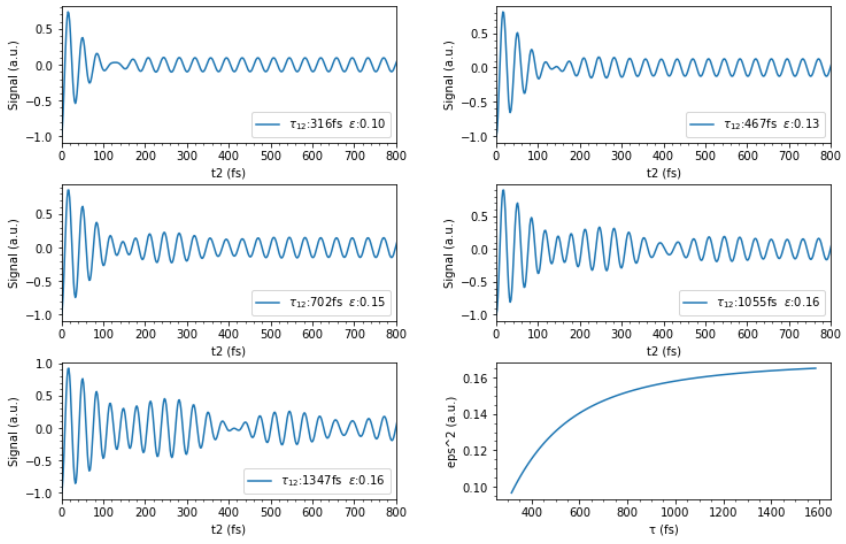

(a)

Figure 3.16: To test the non adiabatic vibronic model the inter exciton coherence time τ_{12} has been varied an the resulting stimulated emission residuals were recorded. In the bottom left corner the coupling strength, ϵ, is plot τ_{12}. For high enough τ_{12}, a beating figure on the dynamics appears, therefore to be able to experimentally see the beating figure the experiment design has to focus on erasing any incoherent interference so that the coherent state between exciton could last longer.

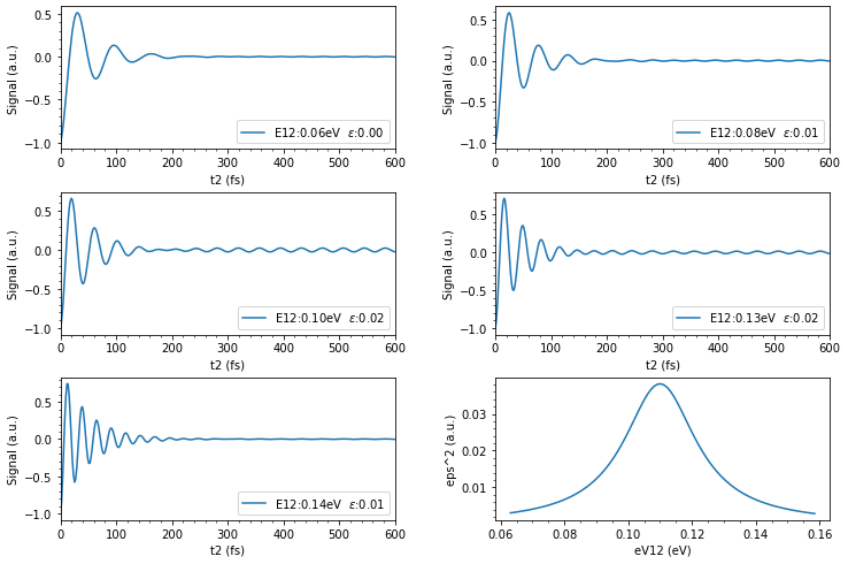

(a)

Figure 3.17: Similarly to Fig. 3.16, the E12 energy gap has been varied to measure the impact of the quasi resonance condition on the residual dynamics and on ϵ

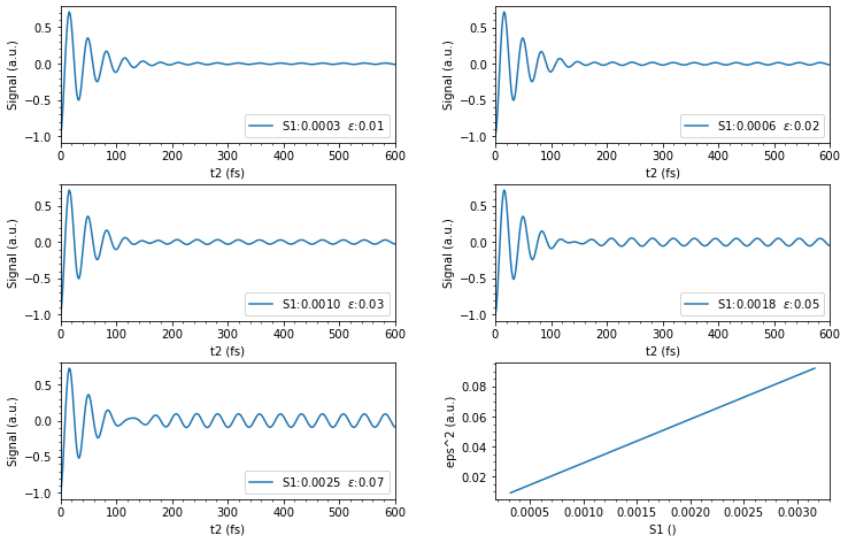

(a)

Figure 3.18: At last, the vibronic coupling Huang-Rhys factor S_1 was varied to measure the impact of the coupling strength upon the long lived oscillation. Indeed the oscillating character vanishes very soon if a weaker coupling is in place.

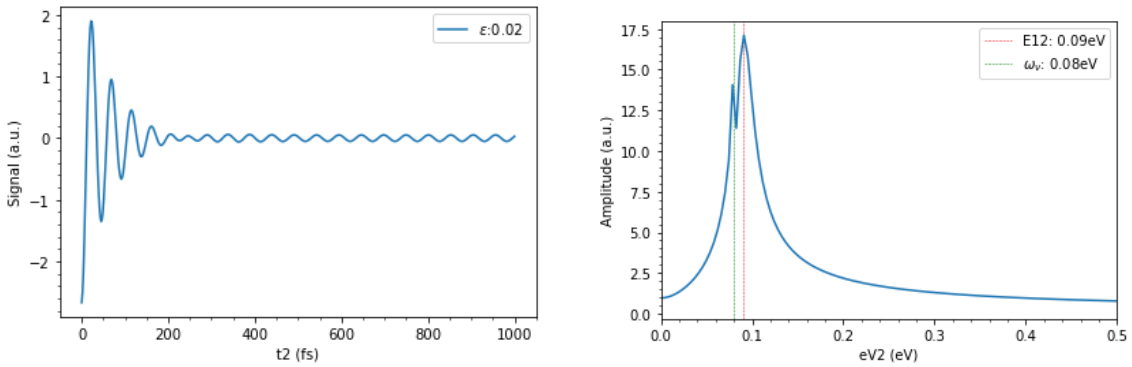

(a) (b)

Figure 3.19: As a didactic exercise the experimental data presented in the article [25] has been successfully replicated. Parameters were set as following: $E01 = 1.8eV E12 = 0.09eV \omega_\nu = 0.08eV S_1 = 0.0006 \tau_{12} = 417 fs \epsilon^2 = 0.02$. The residual dynamics of the stimulated emission signal in (a) and the Fourier transform amplitude in (b).

Pure nuclear vibrational modes are not the only possible way for a molecule to show oscillation in the response function. Electronic coherences and Rabi's oscillation are examples of pure electronic vibration processes that have nothing to do with a mechanical oscillation of the nuclei, they are in fact pure quantum phenomena. In very much controlled and isolated systems, namely coherent systems, those oscillation can be experimentally measured. Being at ambient temperature condition and within weakly interacting environment is usually enough so that coherency is quickly lost making pure coherent oscillation hard to detect. The existence of electronic coherences has though different way to affect experimental results, therefore its modeling has been proven to be successful in explaining oscillating 2DES signals of complex system at environmental temperature condition[25]. First motif of the following paragraphs are the results contained on "Vibronic origin of long-lived coherence in an artificial molecular light harvester", an article published in 2015 on Nature Communications by J. Hauer and colleagues [25]. The claim of this work is to relate measured long-lived oscillation to a vibrational-electronic coherent coupling. This kind of interaction is often called Vibronic to highlight the interplay of both electronic and nuclear states and the mixture nature of the eigenstates of the resulting Hamiltonian. The interplay comes from a quasi-resonant condition of a vibrational replica of an electronic excited state with an higher energy electronic state. The resonance opens the possibility of an interaction of the two involved states, leading in certain condition to vibronic and vibrational coherences that can be measured, according to the above cited article, as long-lived beating signals in 2D spectra. In the documentation of the article theoretical supporting arguments are presented, and the simulation

presented in this current work incorporates the response function's proposed equations to replicate the experimental result. The article includes the analysis for different signals coming out of a "macroscopically aligned tubular system in a polarization-controlled 2D spectroscopy" [25] experimental set up. Differently, the following paragraphs neglect the light-polarization dependence bringing focuses only on a diagonal peak, referred as N11 in the cited article. Even though, coming from an experimental side makes very hard to perform the analysis separating between stimulated emission signals and photo bleaching one, the individual contribution it is crucial since only the excited state vibronic coherence can enhance exciton transport [25](jurgen, 37). Further and more complex simulation could in fact separate this signal guiding the distinction on experimental data. Differently from the approach used until now, the dynamics generated and shown are not coming from a whole-spectrum simulation. The spectra along detection and excitation axis are thus not computed and the response function signals that will be shown are for now only variables of t_2 . This makes the simulation incomparably more quick but also it prevents unexpected interplay between each of Hamiltonian contribution independently add to the model. In the end, a more general analysis is brought to attention in order to again explore the model capabilities and to show possible new phenomena introduced by the model.

In this paragraph a replica of the experimental signal presented in "Vibronic origin of long-lived coherence in an artificial molecular light harvester" is shown. Starting from the article equations and the parameters value are set accordingly to the article, and approximations are introduced based on the same experimental evidence. The parameters involved are then:

- the frequency of the pure vibrational mode, expressed by ω_ν [eV]
- the pure 1-2 exciton decay rate, expressed by τ_{12} [fs]
- the Huang-Rhys factor of the coherence in the exciton base, also referred as effective Huang-Rhys factor, expressed by S1 [ ]
- the energy gap of the first and the second excited states, expressed by E12 [eV]

Firstly the energy splitting introduce by the coupling is set to zero and so the coupling introduced difference in the pure vibrational decay rate is neglected. This first two simplification are supported by a weak coupling hypothesis, in fact for a coupling factor epsilon defined as:

$$\epsilon = i\omega_\nu \sqrt{S_1}(i(\omega_\nu - E12) - \frac{2\pi}{\tau_{12}})^{-1} \tag{3.3}$$

ϵ is supposed much smaller than 1, theoretical estimation of this two quantities are of the order of 0.0001eV that it is below the experimental energy resolution of 0.005eV. In the simulation such resolution is lowered by taking a longer time evolution span, but the same approximations have been introduced with the aim of better reflect the same dynamics of the signal. An additional simplification, supported by the same argument, is that pure vibrational decay rate itself is set to zero. The estimated value for this time constant is bigger the 1 ps, a time interval longer even of the one employed in simulation environment. The simplified response function for a fixed pair of detection and excitation energy, it is given by:

$$R(t_2) \propto \exp(iE12 - \frac{2\pi}{\tau_{12}})t_2 + \epsilon^2 \exp(i\omega_\nu t_2) \tag{3.4}$$

Setting the remaining parameter as the one experimentally measured taken from the source article, the same dynamics with its relative transform amplitude are shown in Fig.3.19b. As can be noticed, the vibrational dynamics in Fig.3.19a does not look like the one shown in the past section. The oscillation starts intense but after a short time related to τ_{12}, such intense contribution fades out leaving a long lived smaller vibration that the article refers to as a beating signal. The beating nature of the signal becomes clear focusing the attention around the time interval during which the system changes oscillation regime. Around the 200 fs mark in the map in fact a distinguishable beating figure is in fact present. Further simulations, that will be later presented, shows such beating to be dominant for bigger exciton coherence time constant. This complies with theoretical arguments and predictions, but it also clarifies why such beating is so hard to detect experimentally. The transform plot at side shows a neat spectrum where the quasi-resonance condition is met. The weak-coupling hypothesis, epsilon squared being around 0.02, makes those peak of unbalanced intensity. In fact the exciton peak, at slightly higher energy, is much wider and intense, but as seen in the dynamics plot also very short-lived compared to the pure vibrational mode.

Beside replicating the article's plotted dynamics, holding as true the same assumptions of the previous discussion, three parameters are being varied in order to discuss different system's scenarios and to characterize the relation between parameters and dynamics changes. The three selected parameters are the Huang-Rhys factor S1, the exciton coherence decay time constant τ_{12} and the central energy of the 1-2 exciton, E12. Even though the previously introduced parameters might still play a role, their impact has not been investigated because as stated the simulations developer for the vibronic description were not comprehensive of all the previous models. No 2D spectral map has been produced, so no lineshape dynamics has been characterized in terms the newly added parameters. Adding a vibronic coupling term to the comprehensive model Hamiltonian would also give

an overall response function that has been not derived and that it would be different from just a product of the previous. The first parameter to be discussed is the Huang-Rhys factor, Fig.3.18. S1 sets the strength of the coupling as it enters ϵ 's definition. In the simulation, the only appreciable effect concerns the amplitude of the long lived vibrations. ϵ^2 is in fact shown to be linear dependent in S1 and the long time limit of the Response Function in Eq.3.4 also suggests a simple linear dependence of the oscillation amplitude in respect to epsilon squared.

The second parameter analysis results are shown in Fig.3.16. Increasing τ_{12}, physically means increasing the coherency life span and thus the coupling with the nuclear vibrations. Moreover in Fig.3.16 a non trivial relation between τ_{12} and epsilon it is noticed. What it is mostly noticeable it though the beating effect that grows with τ_{12}. The explanation for this is related both to the an enhanced coherence life time and an empowered coupling strength, but the consequences are much more dramatic that the effect of S1, which was as well increasing epsilon. Best way to understand such consequences is looking at the equation of the response function as a weighted sum of two the quasi-resonant sinusoidal. Only if the weights are comparable the beating show itself as a low frequency modulation on the top of the original frequency. Pure vibrational sinusoidal is weighted by the constant epsilon, the pure exciton coherence sinusoidal is at opposite weighted by a decreasing monotonic time dependent function. A t close to zero exciton oscillations are dominant, whereas after long time that same oscillation has been long expired. For every choice of the parameters there is time interval where the two amplitudes have roughly the same value. During that time interval the beating is noticeable and a bigger $\tau 12$ enlarges in fact that interval reducing the decreasing rate of the exciton oscillation's amplitude. Not all physical system shows such long coherence life time, thus measuring such clear beating is very complicated and probably out of discussion for organic molecule at room temperature.

The last parameter to be individually analysed is the energy gap between the first two excited states. The value controls directly the off-resonance detuning, but in respect of the vibrational tone energy it only affects the resonance condition. E12 enters epsilon's definition only once, compared to ω_ν that does it twice. The most straight forward effect, to be noticed and explained, is the change in frequency in the short time limit oscillation. Within the short time limit coherence exciton oscillations dominate the signal's overall dynamics and this the frequency change reflects it. As a matter of fact, the same cannot be said in the long time limit. The frequency does not change while the amplitude reaches its maximum when the system meet the resonant condition and becomes dimmer for higher or lower energy gap values. Epsilon squared, that regulates the long time limit

amplitude of the oscillations, shows in fact the same parametric dependence in respect to E12. Therefore oscillations at long time do comes from the vibrational mode but, within a vibronic coupling framework, such mode contribution survives only close to resonance.

This analysis concludes the pure simulation results of this work. In the next chapter, the developed tool and the knowledge acquired will be validated applying them to an experimental data set. In this way it will be possible to evaluate the applicability and the usefulness of the simulated models and design further implementations to best replicate all kinds of experimental signals.

4 | Experimental and modeling results:

In this chapter a brief discussion of the DBOV 2DES experimental result will be given. The experimental evidences work in fact as the basis on which the simulation is built. The comparison between the real and the simulated data shows a good match of the two, so that the experiment conclusions could be strengthen by the simulation analysis.

4.1. Sample introduction: Nano graphenes and DBOV

Nanographenes (NGs) and graphene nanoribbons (GNRs) are carbon compound with a quasi zero dimensional electron confinement. The structure of such material can be completely engineered in term of length, width and edge structures with excellent results in terms consistency and regularity of the synthesis product [26]. While nanographenes used be obtained as cut-outs from a full graphene sheets, new advanced bottom-up synthesis technique have been proposed in recent years with promising success in atomic precision functionalization. Out of this broad class of molecules, Dibenzo[hi, st]ovalene (DBOV) shows excellent properties including strong fluorescence and high ambient stability [27]. Moreover DBOV has been proposed as gain medium for lasing and as active material to achieve strong exciton-photon coupling in micro cavity [1][28]. The optoelectronic properties of this particular type of nanograhene structure, have been investigated to characterize the role of the molecule dimension, internal doping and peripheral substituent. The experiment presented here is only one of many characterization of the chemical and photo physical properties of DBOV with different substituents.

This paragraph will give only a compendium of the published results presented in literature of such characterization. The first kind of tunability of nano graphene optical properties comes from the shape factor of the molecule and the Zigzag edge[29]. The referenced article investigated such effect in different shaped [n,m]peri-acenoacene. In that case a longer zigzag edge is measured to cause a red shift in the stimulated emission signal and a sensitive diminution of the lasing threshold. This tendency is maintained up to a certain

edge length after which the stimulated emission splits and seems to be quenched by an overcoming photo induced absorption contribution. A blue shift is instead obtained doping a DBOV with hetero atoms. In the particular the case of 1,2-Oxaborine doping shows a shift towards smaller wavelengths when an atom of oxygen and one atom of Borine are added inside the nano graphene cyclic structure[30]. Other kinds of properties modulation can be shown as peripheral substituents are added the the DBOV molecule. A change in lasing capabilities [1], organic solvent solubility [1] and within the pump-probe lineshape inhomogeneous broadening[30] has been found for various DBOV derivatives obtained by different substitution patterns.

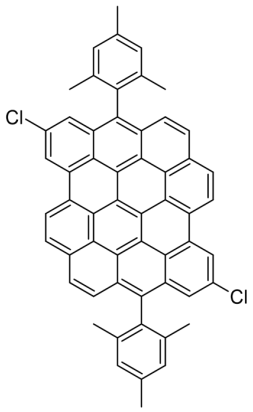

Figure 4.1: DBOV-Mes-Cl, Mes substituent to control the solubility in organic solvent whereas Cl modifies the optoelectronic properties

This streak of experiments helped to investigate the DBOV application capabilities, in the same time a better understanding of nano graphene was reached and new curiosity raises especially about the possibility of combining different functionalized DBOV derivatives. In this sense the nano graphene used in this experiment, namely the DBOV-Mes-Cl in figure 4.1, was chosen upon its high organic solvent solubility given by the -Mes substituent in R1 position and the new characterization possibility given by Chlorine atoms in R3 positions. As a matter of fact in the above cited experiments, the peripheral functionalization was added only in R2 position, the so called bay position. For such molecule, 2DES experiment represents a great tool for the molecule characterization. In fact, as it will be shown, DBOV-Mes-Cl shows an oscillatory dynamics with a period of about $150fs$, therefore the sub $20fs$ temporal resolution represents the only viable way to measure such signal. Additionally, as it was argued in the second chapter, 2DES spectra let distinguish between excitation state mode and ground state one.

4.2. Experimental results:

The experimental characterization of the sample lays on the combination of different experiments, some of them previously performed in the same ultrafast laboratory at Politecnico di Milano by PhD Rafael Muñoz-Mármol. For all the experiments DBOV, being highly soluble, is mixed in liquid-phase solution of Toluene ($C_6H_5CH_3$), a colorless organic solvent commonly used for this purpose.

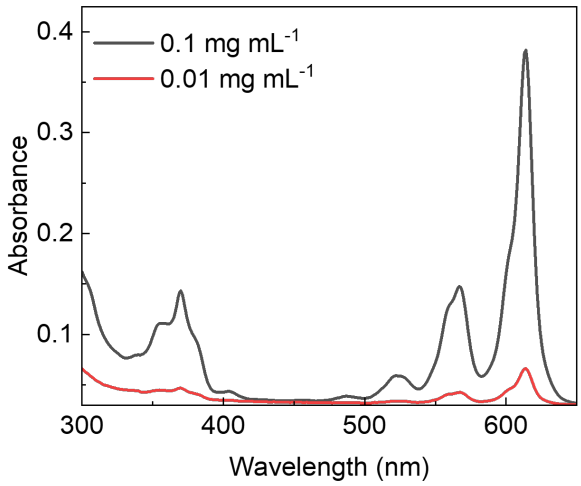

Figure 4.2: DBOV linear absorbance spectrum

To first characterize the sample and guide the further investigation, the linear absorption spectrum was first measured, as in Fig.4.2, for different concentration. Focusing in the visible region (540nm-660nm) the spectrum shows one main peak around 628nm (1.975eV). From the peak profile, vibrational replicas can be spot at different energy intervals. The Pump-Probe dynamics at Fig.4.3, three vibrational modes could be measured. The most energetic causes the dimmer replicas in Fig. 4.3a, and the other two are noticed when taking the Fourier transform of the t_2 dynamics as in Fig. 4.3b. The coexistence of the two most energetic modes has direct evidence in the 2DES experiment results, in Fig. 4.4 and 4.5, more thoroughly discussed in next paragraphs.

First column of Fig. 4.4 shows the evolution of the experimental 2D spectra of DBOV. The cross peaks are in fact proof of an interplay between an energetic vibrational mode and the electronic transition. As a matter of fact, if the vibrational modes were there but no vibronic coupling was, pumping the sample in the visible spectrum would not be effective in probing the vibrational states. Lineshape of the main peak is quite steady and this suggest a very short correlation time but also the presence of a very much spread negative

contribution, caused photoinduced absorption, that quenches all the weaker feature the map might have shown. A photoinduced absorption process seems of taking place for a combination of excitation energy equal to 1.85eV and a detection energy equal to 2 eV. A particular result of such experiment is presented in Fig.4.5. The oscillation in the dynamics are in general so clean that an almost perfect counter phase relation is noticed between dynamics of points taken across the peaks. This effect is particularly clear for the peaks at $eV_{probe} = 2.01eV$, but including in the discussion the peak above and below such energy , respectively Fig.4.5d and Fig.4.5e, highlight another aspect. As it has been point out in the last chapter, cross peaks have a dominant character that is either of ground state as the one in Fig.4.5d or of excited state Fig.4.5e. The figures differ strongly in the amplitude of the oscillation shown, this is a clear argument for a stronger coupling between the excited state and the vibrational mode responsible for the oscillation visible in the figure. Simulation results will further investigate about such statement, clearing if this diversity in coupling could be explained by the adiabatic displaced oscillator model or not.

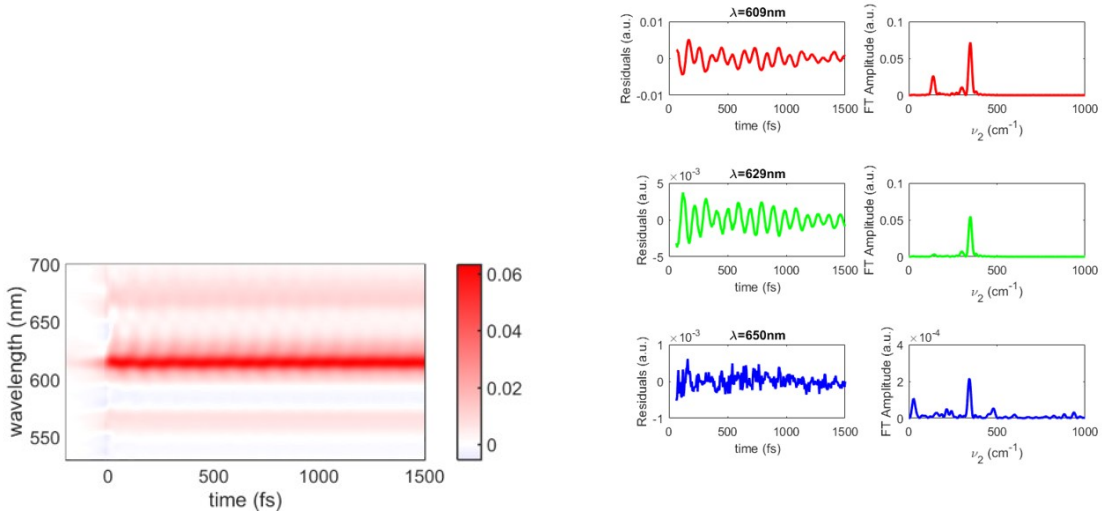

(a) (b)

Figure 4.3: Two pulses pump-probe data offers the starting benchmark for designing a 2DES experiment. With the due conversion from wavelength and energy, main peak position and vibronic replicas can be extract from the pump probe map (a). As for the dynamics and the Fourier transform amplitude in (b), they were useful for the modeling as the relative amplitude of the vibrational modes appears clear.

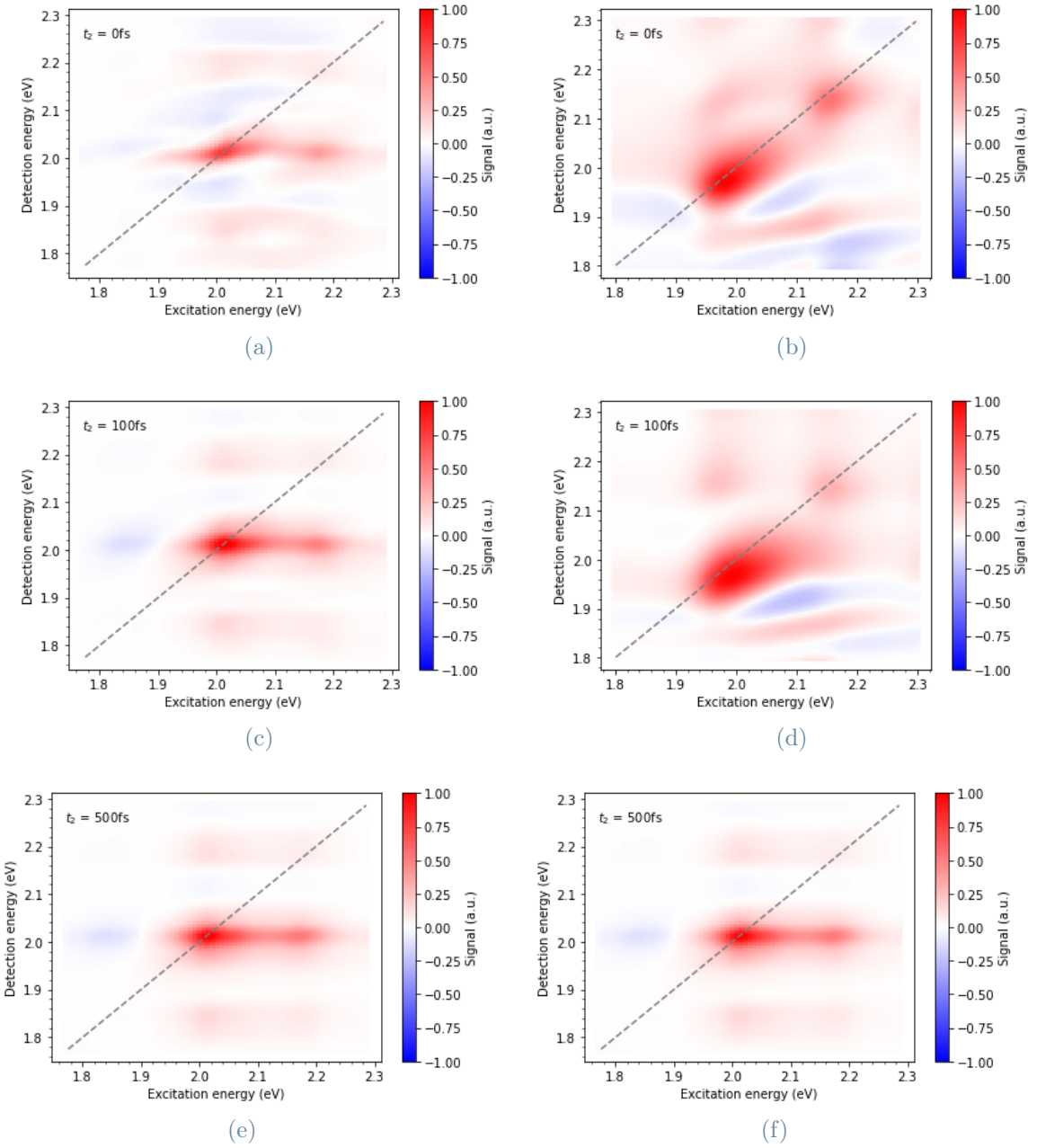

Figure 4.4: Experimental and simulated maps in a matching comparison. (a),(c)(e) are the DBOV experimental maps at different time instants, while (b)(d)(f) the fully simulated ones. For the simulation the parameters were set as: $E01 = 2.01eV \tau_C = 80fs \lambda = 0.05eV z_1 = z_2 = z_3 = 1\tau_V = 10ps \omega_{\nu 1} = 0.18eV \omega_{\nu 2} = 0.04eV \omega_{\nu 3} = 0.01eV Amp_{\nu 1} = 1.7Amp_{\nu 2} = 0.8Amp_{\nu 3} = 0.3$. The result shows some matching characteristic as the cross peaks position and the overall broadening. The photo-induced absorption experimentally measured is out of the model capabilities since all the simulation were base on a two level system.

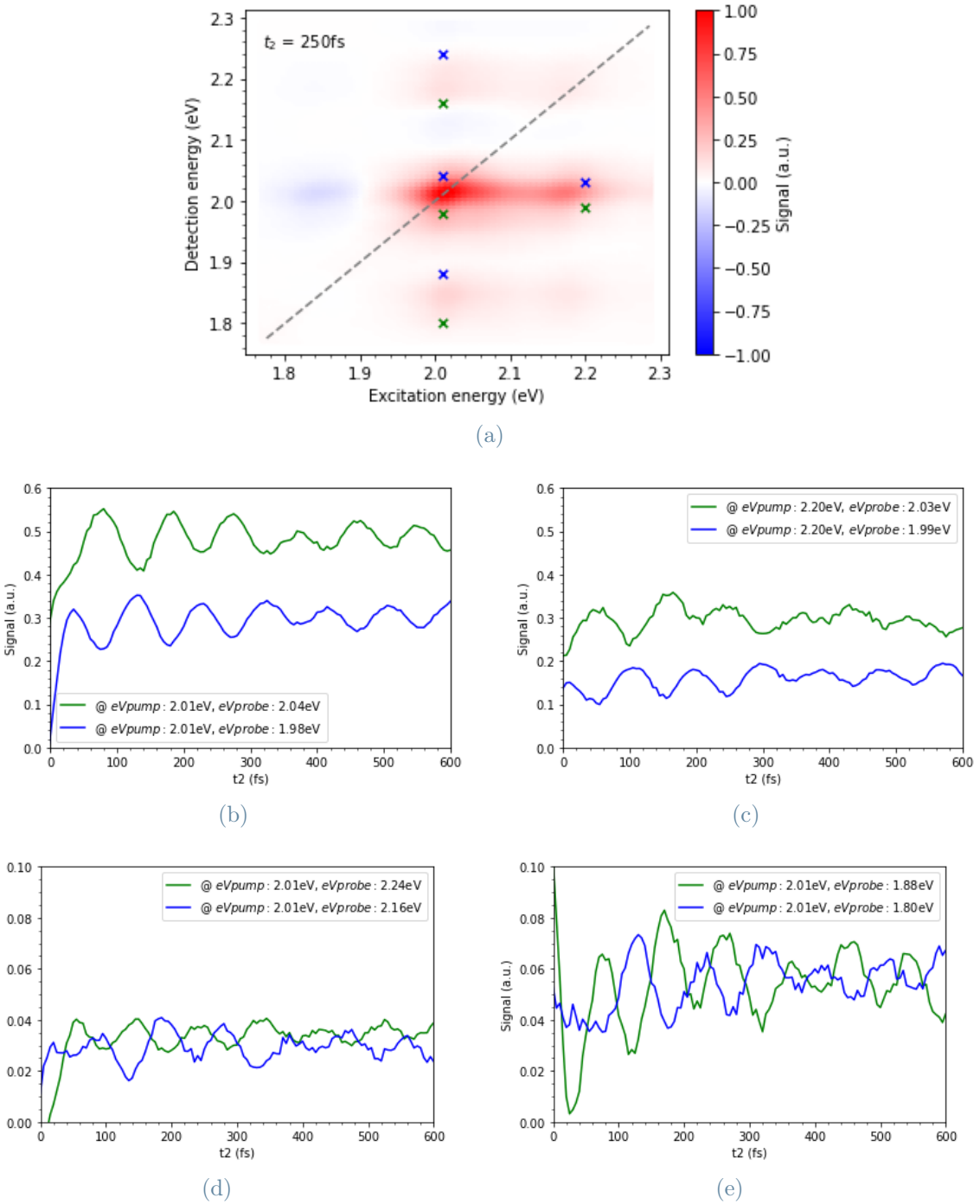

Figure 4.5: The counter phase relation across peaks have been studied with success for the DBOV experimental data. (b) contains dynamics taken across the diagonal peak, (c) the ones taken across the cross peak at higher excitation energy, (d) the ones taken across the cross peak at higher detection energy, therefore of ground state character, and (e) the ones taken across the cross peak at lower detection energy, therefore of ground state character

4.3. From experiment to simulation:

This section aims to derive from the experimental knowledge, a choice for the model to be use, and the parameter for the simulation to replicate the data. In this way, more insights could be revealed and optoelectronic properties could be better quantitatively characterized. The oscillating dynamics of the signal along the population time strongly suggest the introduction of vibrational modes within energy levels involved in the interaction. The model will thus involve both electronic and vibrational states. In addition, in the system Hamiltonian, a vibronic coupling should be probably introduce. Even though the oscillations do not show any clear beating nature, a possible involvement of non adiabatic term is not to be excluded and it is supported by the long living nature of such oscillations. As it has been shown at the end of the former chapter even for short lasting electronic coherence, the quasi resonance condition between higher electronic energy gap and the vibrational mode is sufficient, in a coupled system, to support a long lasting oscillating signal. Nevertheless to ensure the possibility to simulate the whole 2D spectra and its evolution, the experimental data will be simulated through only pure electronic vibrational terms. Combined with the lineshape evolution description, the aim of the simulation is to replicate the 2D maps at different time instants and the dynamics along t_2 of determined coordinates that show in pairs a counter phase relation. As the experimental plots at figure 4.5 show, the simulated oscillating dynamics of a pair of points having the same excitation energy and detection energies taken across the main peak are expected to show a phase factor of π in respect to the other.

The lineshape model and parameter are retrieved from the experimental condition and the 2D spectra. At first, temperature must be set at laboratory ambient condition of 298K. Secondly the evolution of the lineshape suggest the use of the Brown oscillator model, thus the remaining parameter to set are the reorganization energy, λ, and the correlation time, τ_c. The analysis shown in the former chapter guides the parameter derivation from the 2D maps. Starting with the correlation time, it has been shown how τ_c regulates the time constant of the evolution of the lineshape. The maps at figure 4.4 show a quickly resolved lineshape evolution: both the spectral diffusion and the stokes shift reach their long time limit after about $100fs$, no clear change in the main peak can be after such delay inferred. τ_c is then fixed, below the $100fs$ threshold, at $80fs$. Fixing the correlation time constant, the reorganization energy λ has to be chosen to comply with two condition, the stokes shift value and the amplitude of the lineshape broadening. The most straight forward way to correlate the value of λ is the relation with the stokes shift measured in the maps. For the DBOV-Cl maps, the only evidence that one can use to retrieve a value

for the stokes shift is the larger broadening toward lower detection energy of the main peak. Such asymmetry can be quantified from the experimental maps to be about 10 nm around the peak detection wavelength of 615 nm, this interval translated in energy corresponds to about 0.05eV. Such value has been in fact used as first supported guess for the parameter λ. There is in fact a third condition that has the combination of λ and τ_c has to comply with. The overall uncertainty on the transition energy gap value depends in fact from both parameters and it shows its self on the 2D experimental spectra with a broader or tinier lineshape area. The effectiveness of the model can be then assessed noticing that the overall lineshape area are in fact comparable between experimental and simulated 2D spectra. For the comparison quantitative parameter like the main diagonal full width half maximum value an be used. Looking at figure 4.7, the diagonal's cut FWHM value is about 0.1 eV centered at main peak energy at about 1.95eV. The peak of simulated map is than red shift of about 0.05eV, nevertheless the width of the cut is compatible with broadening within the experimental maps. Once the parameter of the lineshape function have been fixed, the modeling could then proceed to its vibrational part where vibrational modes and their reciprocal amplitude will be discussed.

Starting with the experimental evidence, the frequency analysis of the pump probe data along the t_2 axis, figure 4.3a , highlights the existence of two main vibrational modes. The less energetic mode is found to have an energy corresponding to $140cm^{-1}$ while a more energetic one is found at $350cm^{-1}$. The Fourier transform of the peak's t_2 dynamics, figure 4.3a, gives information on the reciprocal intensity of the modes, it is in fact shown the latter mode having almost three times the amplitude of the former. Those two modes are then added to the model, fixing to 0.017 eV and to 0.043 eV their respective quantum of vibrational energy. Two arbitrary amplitudes are then fixed so the ratio is about one third, for this case parameters $Amp_{\nu 2} = 0.8 Amp_{\nu 3} = 0.3$ are set. With this two modes, one should expect looking at the 2D spectra cross peaks for each vibrational replica. In the experimental maps, the cross peaks are indeed visible but the energy shift from the main peak is totally incompatible with either of the two modes. As the analysis of previous chapter has shown, the cross peak's energy difference corresponds exactly to the value in energy of the quantum of excitation of the vibrational mode. In the experimental maps such energy difference corresponds to 0.18 eV. This energy value is quite beyond the experimental frequency resolution power. The complexity of the measure puts a constraint to the number of maps, namely the number of t_2 instants sampled, and thus the maximum frequency resolved along t_2 is smaller than the one for the t_1 and t_3 axis. The simulation environment overcomes this complexity and the frequency resolution power has been brought up to 4236.1 cm-1 (0.525 eV) making the

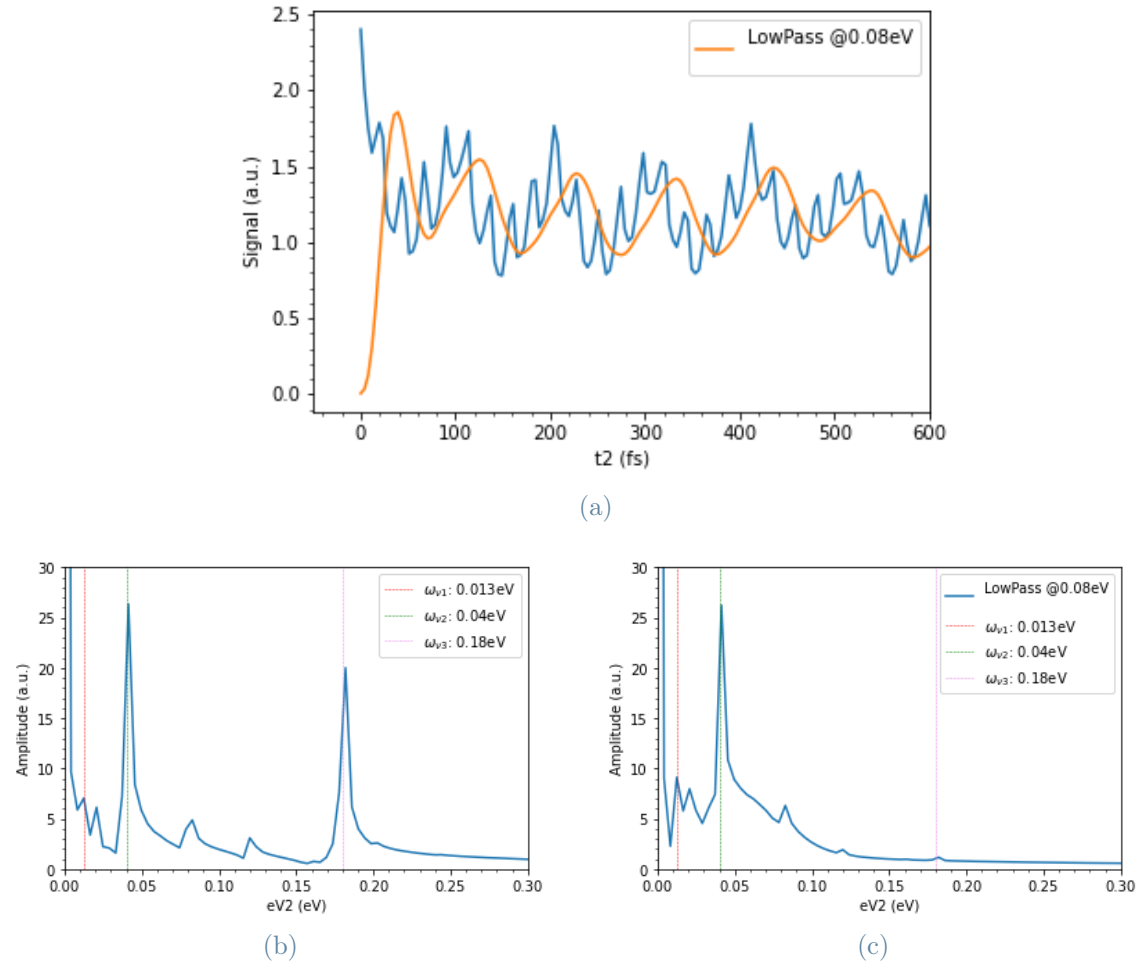

(a)

(b)

(c)

Figure 4.6: Beside the maps, the model simulated also the t_2 dynamics and their relative Fourier transform. (a) shows dynamics of main diagonal peak, because of the much higher frequency resolution power the simulated signal had to be filtered through a low pass to resemble the experimental restraint. The effect of the filter is presented in (b) and (c) comparing the amplitude spectrum of the two signals. The lower energy modes are nonetheless present with an amplitude ratio compliant with the experiment

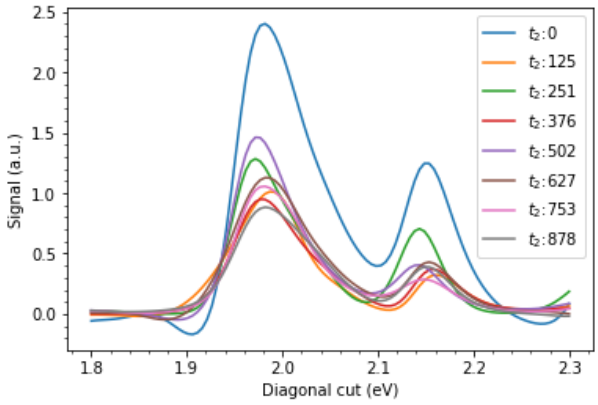

Figure 4.7: Diagonal cut of the simulated 2D spectra t_2 time instants

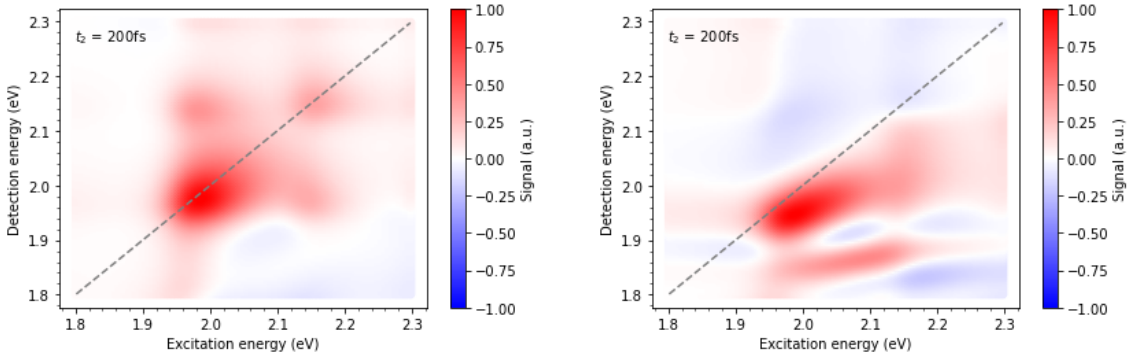

(a) (b)

Figure 4.8: The simulation allows to distinguish the photobleaching cross peaks (a) from stimulated emission ones (b). Despite being overlapped for diagonal peak, the same could be said about cross peaks at different detection energy. Photobleaching cross peaks look also much more ordered and static, a dimmer oscillation of the photobleaching could be in fact highlighted also for the t_2 dynamics.

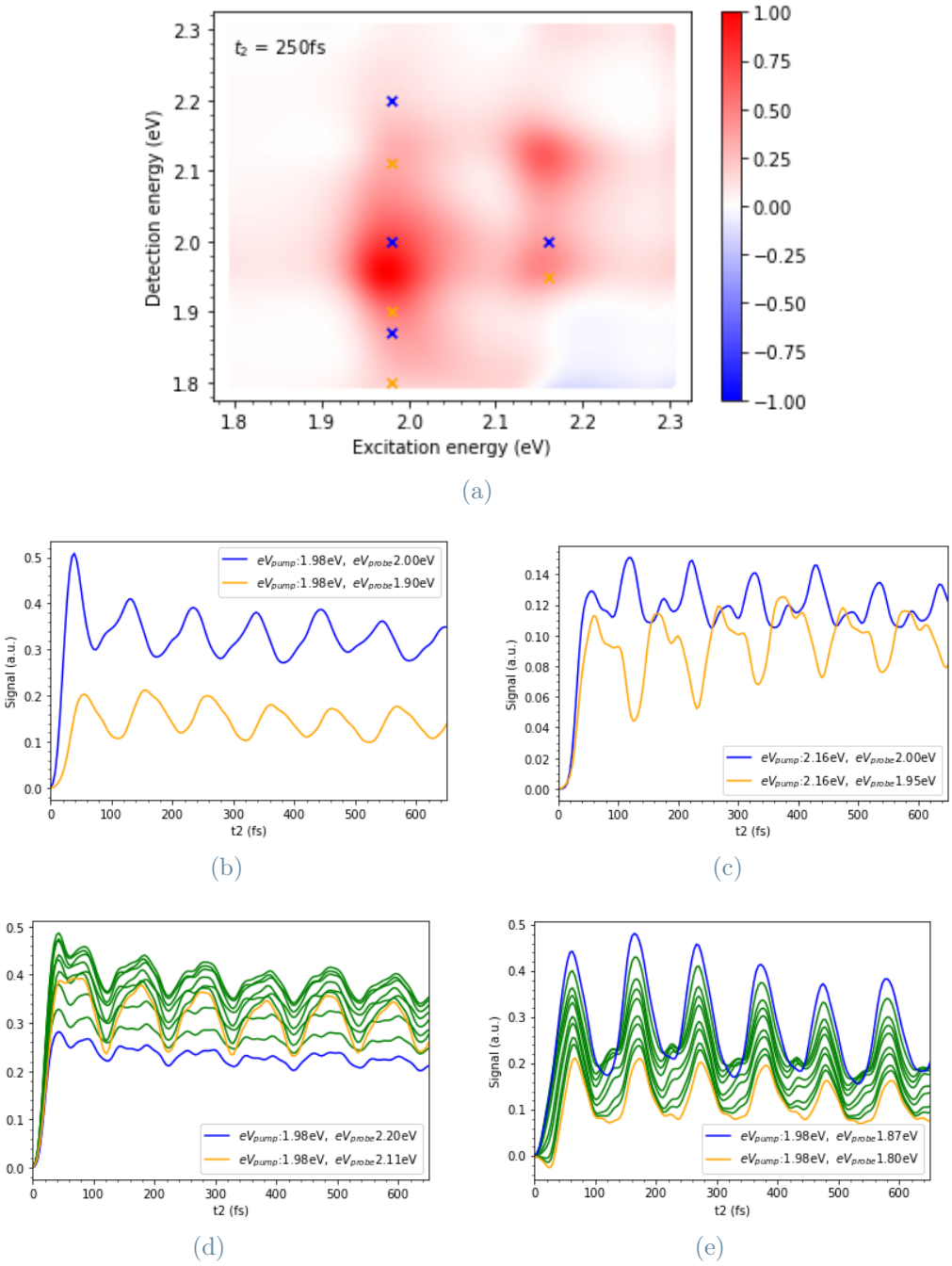

Figure 4.9: The counter phase relation, found within the experiment, was much harder to find between the simulated dynamics. (b)(c) contain the comparison for the points at main peak detection energy. They are therefore mixed nature cross peaks and for them the counter phase relation shows itself clearly. (d) contains the dynamics taken in the interval across the photobleaching cross peak. As it is clear almost no phase factor is retained crossing the overtone pole. The same happens for the stimulated emission cross peak (e). One noticeable difference stands in oscillating amplitude: the mode responsible for the oscillation, $\omega_{\nu 2} = 0.04eV$, has a dominant excited state nature.

vibrational mode at 0.15 eV well resolvable. In this case a third and much more energetic mode is introduced in the model, introducing contextually the cross peaks in the position suggested by the experimental maps. Theoretically, cross peaks can be justified by many different processes and interactions, electron delocalization and exciton coupling are only two example of them [31]. In the simulation presented, the vibrational cause is the only investigated path, but no strong counter evidence has been found.

Having introduced the three vibrational modes with their respective amplitude adjusted, the model was made running to simulate the data. Fig.4.4 contains both the real and the simulated maps. The claim resemblance is based on the lineshape evolution and foremost in position of the peaks, the main diagonal one as well as the cross peaks. The cross peaks correspond in fact to the energetically viable transitions between the two electronic states while at different vibrational excited states. Therefore matching the cross peaks characterizes the molecule quite well.

Further investigation are then brought ahead selecting the main peak as an example over which plotting the t_2 dynamics and its Fourier transform. Figure 4.6a contains the representative graphs. Having introduced the high energy mode, unresolved by the laboratory set up, makes the extracted raw dynamics very different from its experimental reciprocal. This explanation is also supported by the Fourier transform amplitude graph of the unfiltered signal 4.6b. Differently from the graph at 4.3b, the simulated signal shows a major contribution from the component at $0.15eV$. A low pass filter with a energy cut of $0.1eV$ is thus added to the simulation algorithm, this replicates the lower sampling rate of the experimental set up, compared to the one used for the simulation. Doing so, the filtered signal's transform amplitude much more resembles the experimental one and the two lower energy modes and their over tones can be recognized. Such a closer resemblance can be recognized subsequently also looking at the time representation of the filtered signal dynamics, in figure 4.6a.

From the single dynamics comparison, one interesting aspect is last to be verified. The experimental data, thoroughly described in the previous section, manifests an peculiar aspect in the phase relation between dynamics of 2D spectra points across the resonance peak. The model employed it has been demonstrated, in the simulation analysis chapter, to be fully comprehensive of such phenomenon. The aim is to replicate the results in the DBOV simulated spectra. As discussed above, the evidence of such natural phase relation could be easily ruined by the complexity of the system response function. Highlighting the same phase relation of the experimental dynamics graph has indeed been much more complex that the simpler previous chapter case. The results are conveyed in figure 4.9 and nevertheless the paired dynamics in Fig. 4.9b and Fig.4.9c do exhibit the expected phase

relation. To be able to find these results, the dynamics have been simplified with the use of the same low pass filter discussed before, but as it can be retrieved from the map at figure 4.9a the points have been taken more far apart than the experimental case. For the other two couple of points in Fig. 4.9e and Fig.4.9d the counter phase relation could be inferred, in fact scanning for different points across the cross peaks no phase shift can be noticed. In this work no satisfying reasoning could be formulated for this. A confirmation of the experimental results comes instead from the comparison of the oscillating amplitudes. The model employed reflects indeed a difference in coupling between the excited state and the ground state. Fig. 4.9b and Fig.4.9c confirm the subsistence of the counter phase relation despite the complexity of the transform phase function, additionally one could verify that the same phase shift happens across the excitation axis resonance point. This can be first hand proven comparing the same color coded signals of Fig.4.9b and Fig.4.9c. The phase change across the resonance is indeed a very general property of oscillating dynamical systems.

Ending this chapter, a renovated emphasis to the effectiveness of modeling and simulation is due. With the use of a fairly simple adiabatic model, rich and complicated experimental results have been predicted and simulated. Such an approach helps to disentangle the density of information underneath every 2DES experiment. When any models' conflicting hypothesis have been taken care of, a modular architecture can be adopted so that the molecular description follows one simple and yet composed set of rules and interactions. In this sense the implemented model should be generalized for three level systems and including more interaction Hamiltonian terms.

5 | Conclusion:

The results of this Thesis stands on the nanographenes research field and in the scientific modeling and simulation area. A nanographene DBOV derivative was characterised by use of a detailed 2DES analysis. Such analysis contributes to advancing the understanding of vibronic interactions and their potential role played for designing materials with tailored functional properties. By studying the transient 2D spectra, not only the capabilities of 2DES were shown, but also DBOV electronic and vibrational structure has been characterized with a focus on the interplay of the two kinds of degree of freedom. The study argued for a greater involvement of the excited state to the vibrational mode in the respect to the ground state. This can have profound implications in processes like energy and charges transfer within the molecule. Supporting arguments for a different involvement came from the experimental data and from the comparison with simulated data. Such different involvement it is claimed to be caused by the relative displacement of the electronic states in respect to the nuclear coordinates. Such a displacement it is responsible for the oscillation of the response function in respect to all of three time axis and thus for interplay between electronic and vibrational excitation. The simulation of the spectral diffusion of the signal and the Stokes shift were possible adopting a stochastic approach to account the interaction within the sample and the environment. Doing so it was possible to conclude that for the DBOV-toluene solution system such interaction has a short lived auto correlation function and that the amplitude of fluctuations occurred were of orders of magnitude less that the electronic energy gap. This is coherent with the apolarity nature of such a solution. A non adiabatic approach was attempted during modeling but the model was not developed enough so that it could be tested or be of use for the simulation.

Eventually different DBOV substituent atoms and geometry could be studied to best engineer the molecule and to understand the effects and interaction behind some properties of interest. Furthermore the high photoluminenscence shown suggests the possibility to achieve the strong coupling regime when the molecule is placed in a microcavity. The possible implications of it demand a further investigation on the topic. Regarding the model and simulation, various additional implementation approaches are possible. The

first logical step is to generalize the vibrational model to a multiple level system. A three level system model was implemented within the Brownian oscillator model, but it was then rejected for being to computational costly when the displaced oscillator model was introduce. Such a choice prevented the simulation to predict the photoinduced absorption signal present in the sample. A further step would be then introducing a non-adiabatic term in the Hamiltonian to derive more general response functions and a more capable simulation environment.

Bibliography

[1] Giuseppe M. Paternò, Luca Nicoli, Qiang Chen, Klaus Müllen, Akimitsu Narita, Guglielmo Lanzani, and Francesco Scotognella. Modulation of the nonlinear optical properties of dibenzo[hi,st]ovalene by peripheral substituents. *The Journal of Physical Chemistry C*, 122(43):25007–25013, 2018.

[2] Shaul Mukamel. *Principles of nonlinear optical spectroscopy*. Oxford series in optical and imaging sciences. Oxford University Press, 1995.

[3] YingLi Niu, ChihKai Lin, ChaoYuan Zhu, Hirobumi Mineo, ShengDer Chao, Yuichi Fujimura, Michitoshi Hayashi, and ShengHsien Lin. Density matrix method and ultrafast processes. *Science China Chemistry*, 2012.

[4] Hamm Peter. *Principles of Nonlinear Optical Spectroscopy: A Practical Approach*. 2006.

[5] Shaul Mukamel. *Principles of nonlinear optical spectroscopy*. Oxford series in optical and imaging sciences. Oxford University Press, 1995.

[6] Hamm Peter. *Principles of Nonlinear Optical Spectroscopy: A Practical Approach*. 2006.

[7] Shaul Mukamel. *Principles of nonlinear optical spectroscopy*. Oxford series in optical and imaging sciences. Oxford University Press, 1995. URL `https://cir.nii.ac.jp/crid/1130000797363520000`.

[8] Shaul Mukamel. *Principles of nonlinear optical spectroscopy*. Oxford series in optical and imaging sciences. Oxford University Press, 1995.

[9] Frank Ernesto Quintela Rodriguez and Filippo Troiani. Vibrational response functions for multidimensional electronic spectroscopy in the adiabatic regime: A coherent-state approach. *The Journal of Chemical Physics*, 157(3):034107, 07 2022.

[10] Hamm Peter. *Principles of Nonlinear Optical Spectroscopy: A Practical Approach*. 2006.

[11] Giulio Cerullo, Cristian Manzoni, Larry Lüer, and Dario Polli. Time-resolved methods in biophysics. 4. broadband pump—probe spectroscopy system with sub-20 fs temporal resolution for the study of energy transfer processes in photosynthesis. *Photochemical & Photobiological Science*, 2007.

[12] Andrius Gelzinis, Ramūnas Augulis, Vytautas Butkus, Bruno Robert, and Leonas Valkunas. Two-dimensional spectroscopy for non-specialists. *Biochimica et Biophysica Acta (BBA) - Bioenergetics*, 1860, 12 2018. doi: 10.1016/j.bbabio.2018.12.006.

[13] M. Maiuri. *Ultrafast Energy and Electron Transfer Processes in Natural and Artificial Light Harvesting Systems*. PhD thesis, Politecnico di Milano, 2013.

[14] Minhaeng Cho. *Two-dimensional optical spectroscopy*. CRC press, 2009.

[15] Peter Hamm and Martin Zanni. *Concepts and Methods of 2D Infrared Spectroscopy*. Cambridge University Press, 2011. doi: 10.1017/CBO9780511675935.

[16] M. Maiuri. *Ultrafast Energy and Electron Transfer Processes in Natural and Artificial Light Harvesting Systems*. PhD thesis, Politecnico di Milano, 2013.

[17] Daniele Brida, Cristian Manzoni, and Giulio Cerullo. Phase-locked pulses for two-dimensional spectroscopy by a birefringent delay line. *Opt. Lett.*, 37(15):3027–3029, Aug 2012.

[18] Giulio Cerullo and Sandro De Silvestri. Ultrafast optical parametric amplifiers. *Review of Scientific Instruments*, 74(1):1–18, 01 2003.

[19] M. Zavelani-Rossi, G. Cerullo, S. De Silvestri, L. Gallmann, N. Matuschek, G. Steinmeyer, U. Keller, G. Angelow, V. Scheuer, and T. Tschudi. *Opt. Lett.*, (15):1155–1157.

[20] Russo Mattia. *Light-Driven Energy Conversion Processes in Natural and Bio-inspired Light Harvesting Systems probed by Two-Dimensional Electronic Spectroscopy*. PhD thesis, Politecnico di Milano, 2022.

[21] https://www.spyder-ide.org/.

[22] František Šanda, Václav Perlík, Craig N. Lincoln, and Jürgen Hauer. Center line slope analysis in two-dimensional electronic spectroscopy. *The Journal of Physical Chemistry A*, 119(44):10893–10909, 2015.

[23] Mattia Russo, Kirsty E. McGhee, Tersilla Virgili, David G. Lidzey, Giulio Cerullo, and Margherita Maiuri. Dephasing processes in the molecular dye lumogen-f orange characterized by two-dimensional electronic spectroscopy. *Molecules*, 27(20):7095, 2022. ISSN 1420-3049.

[24] Edward L Mertz, Vyacheslav A Tikhomirov, and Lev I Krishtalik. Stokes shift as a tool for probing the solvent reorganization energy. *The Journal of Physical Chemistry A*, 101(19):3433–3442, 1997.

[25] James Lim, David Paleček, Felipe Caycedo-Soler, Craig N. Lincoln, Javier Prior, Hans von Berlepsch, Susana F. Huelga, Martin B. Plenio, Donatas Zigmantas, and Jürgen Hauer. Vibronic origin of long-lived coherence in an artificial molecular light harvester. *Nature Communications*, 2015.

[26] Yanwei Gu, Zijie Qiu, and Klaus Müllen. Nanographenes and graphene nanoribbons as multitalents of present and future materials science. *Journal of the American Chemical Society*, 144(26):11499–11524, 2022.

[27] E. Jin, Q. Yang, C. W. Ju, Q. Chen, K. Landfester, M. Bonn, K. Müllen, X. Liu, and A Narita. A highly luminescent nitrogen-doped nanographene as an acid- and metal-sensitive fluorophore for optical imaging. *Journal of the American Chemical Society, 143(27), 10403–10412*, 2021.

[28] David M. Coles, Qiang Chen, Lucas C. Flatten, Jason M. Smith, Klaus Müllen, Akimitsu Narita, and David G. Lidzey. Strong exciton–photon coupling in a nanographene filled microcavity. *Nano Letters*, 17(9):5521–5525, 2017.

[29] Rafael Muñoz-Mármol, Fernando Gordillo, Víctor Bonal, José M. Villalvilla, Pedro G. Boj, José A. Quintana, Aaron M. Ross, Giuseppe M. Paternò, Francesco Scotognella, Guglielmo Lanzani, Amel Derradji, Juan C. Sancho-García, Yanwei Gu, Jishan Wu, Juan Casado, and María A. Díaz-García. Near-infrared lasing in four-zigzag edged nanographenes by 1d versus 2d electronic pi-conjugation. *Advanced Functional Materials*, 31(41):2105073.

[30] Yanwei Gu, Rafael Muñoz-Mármol, Wei Fan, Yi Han, Shaofei Wu, Zhengtao Li, Víctor Bonal, José M. Villalvilla, José A. Quintana, Pedro G. Boj, María A. Díaz-García, and Jishan Wu. Peri-acenoacene for solution processed distributed feedback laser: The effect of 1,2-oxaborine doping. *Advanced Optical Materials*, 10(7):2102782, 2022.

[31] M. Maiuri. *Ultrafast Energy and Electron Transfer Processes in Natural and Artificial Light Harvesting Systems*. PhD thesis, Politecnico di Milano, 2013.

List of Figures

Acknowledgements

This work would not have been possible without the guidance and the enthusiasm of Professor Margherita Maiuri and PhD Mattia Russo. Furthermore I want to thank PhD Rafael Muñoz-Marmol for its support within the interpretation the sample data. Moreover a grateful mention goes to all the members of Cerullo's research group at Politecnico di Milano.

Working on this Thesis has been for me a real opportunity of growth and to meet new aspects of working in research. I want to share this accomplishment with the one I love and care. Among others, to Barry and Jeff.

Progress and technological breakthroughs have been one of the few consistent news we have lately received. In the last decades engineers, scientist and may others have been discovering and mastering all sorts of solutions for all sorts of problems. Nevertheless happiness and well being around the world seems to have much more of a struggle spreading through. The world and society is a complex system: at every scale variables and interactions are too many even to be counted, it is impossible to account for them in deterministic way. For a stochastic description the hypothesis of an equilibrium existence may not be fit, and surely enough ergodicity does not hold. Interpretative models have to be simplified so much and with such arbitrary assumptions that we might call them ideologies or religions. Models are fun to play and a source of gratitude when put in to work. But after all electrons, photons, nuclei and living beings do not behave following any model. It all can be much easier: Ceasefire, Peace.